FORMATION FLYING WITH SHEPHERD SATELLITES

Michael R. LaPointe
Ohio Aerospace Institute
Cleveland, OH 44142

Phase I Final Report
NASA Institute for Advanced Concepts
Grant 07600-072

December 2001

TABLE OF CONTENTS

LIST OF FIGURES

FORMATION FLYING WITH SHEPHERD SATELLITES
NIAC PHASE I FINAL REPORT

Michael R. LaPointe
Ohio Aerospace Institute
Cleveland, OH

ABSTRACT

Formation-flying an array of specialized microsatellites in place of a single, multi-instrumented spacecraft offers several advantages for earth and space science applications. However, the formation and control of a distributed array of several small, power-limited satellites is a tremendous challenge for current guidance, control and propulsion technologies. A new concept is proposed in which a limited number of special service satellites are used to form and maintain a large number of microsatellites in a precise formation. The proposed "shepherd satellite" concept removes the considerable difficulty associated with the positioning and control of individual microsatellites within a formation-flying array, and places that burden on a small number of shepherd satellites that can more easily be controlled through autonomous programming or ground commands. Active maneuvering of the array and the positioning of distributed elements within the array are performed through the shepherd satellites, which allows the individual microsatellites to devote their limited mass and power resources to instrumentation and observation.

1.0 INTRODUCTION

The National Aeronautics and Space Administration (NASA) has advocated the use of small satellites flying in precise formations to enhance or enable a number of Space Science and Earth Science strategic enterprise missions.[1] The advantages of formation flying several small, specialized satellites in place of a single, complex science platform include substantially lower satellite production costs, a distribution of risk across formation elements to reduce catastrophic failures, and enhanced mission flexibility through adaptive formations and low cost replacement satellites. For near-earth applications, the economy of scale provided by the use of small, low mass satellites allows a single launch vehicle to deliver several satellites to orbit, and low cost piggyback launches on other vehicles can be used to replenish satellite clusters. As noted in a recent publication by the NASA Goddard Space Flight Center, "Formation flying is quickly revolutionizing the way the space community conducts autonomous science missions around the Earth and in space. This technological revolution will provide new, innovative ways for this community to gather scientific information, share this information between space vehicles and the ground, and expedite the human exploration of space."[2]

Representative NASA programs that plan to use formation flying satellites are the Space Technology 3 (ST-3) mission (formerly Deep Space 3),[3] which will validate advanced technologies required for deep space formation flying of multiple spacecraft; the Terrestrial Planet Finder (TPF) mission,[4] an ambitious plan to configure several spacecraft into a long baseline interferometer capable of detecting planets in other solar systems; and the Earth Observing System (EOS) programs, which include the current Earth Observing (EO-1) mission, the Earth System Sciences Program (ESSP), the Vegetation Canopy Lidar (VCL) mission, and the EOS/IceSat mission.[5] In addition to NASA, the European Space Agency is planning a number of formation flying missions[6] including the SMART-2 two-satellite test array, the Laser Interferometer Space Antenna (LISA) for gravitational wave detection, and the Darwin terrestrial planet finder array. The U.S. Air Force Research Laboratory (AFRL) is also developing technologies required for satellite formation flying through the TechSat 21 (Technology Satellite of the 21st Century), program, which will employ distributed satellites for terrain mapping, navigation, and communication

applications.[7,8] Farter-term formation-flying concepts supported by the NASA Institute for Advanced Concepts (NIAC) include the Micro-Arcsecond X-ray Interferometry Mission (MAXIM),[9] the Lifefinder telescope project,[10] and ultralight astronomical telescopes and arrays.[11]

While distributed satellite formations offer several advantages over large multi-instrumented spacecraft for earth and space science applications, there are a number of significant technical challenges that must be overcome to transition these systems from concept to reality. In particular, the formation and maintenance of large clusters of tens to hundreds of small, power-limited, 10-kg to 100-kg satellites (generally referred to as nanosatellites or microsatellites) present serious difficulties for satellite navigation, guidance, control and propulsion. Current approaches to meet these challenges include the use of global positioning systems for satellite tracking and navigation, autonomous spacecraft control algorithms to correlate observations and maintain precise inter-satellite separations, and electric or chemical microthrusters to provide satellite station-keeping, drag make-up, and array reconfiguration.[12-24] Each of these techniques, while promising, have inherent limitations that may make their implementation exceedingly difficult to put into practice. Current global positioning systems can keep accurate track of individual satellite and array orbits, but cannot provide the precise location information required by satellite interferometers and cannot be used for spacecraft arrays flying beyond geosynchronous orbit. Closed-loop algorithms for spacecraft control have become remarkably versatile and robust (as witnessed by the success of NASA's Deep Space 1), but to date such algorithms for N-body satellite control remain unproven. Electric propulsion systems, such as pulsed plasma thrusters, can provide the fine control required for drag makeup and station-keeping but will compete for limited spacecraft power. Chemical microthrusters can provide higher thrust than their electric thruster counterparts, but use more propellant due to their lower specific impulse values, resulting in a larger propellant mass fraction or a reduced operational life. In addition, potential contamination of neighboring spacecraft by propellant exhaust plumes and the possibility of pulsed electromagnetic interference with low power inter-satellite communications remain a real concern for tightly grouped clusters. To mitigate these concerns, propulsive conducting tethers and spin-stabilized tether systems have been proposed in place of on-board propulsion systems to form and maintain satellite formations.[25,26] While such concepts offer intriguing possibilities for small arrays consisting of a few spacecraft, implementing a workable system for several dozen satellites quickly becomes problematic.

Although it is anticipated that significant progress will be made over the next several years toward solving the complicated and interlocked set of requirements outlined above, it appears advantageous at this point to consider new and potentially more versatile techniques for spacecraft cluster formation and control. This Phase I final report describes a revolutionary approach that removes the burden of navigation, guidance, and control from the individual satellites in an array and places it onboard a small number of satellites flying on the outskirts of the formation – so called *shepherd satellites* that keep a distributed flock of small specialized spacecraft in their appropriate array locations. By placing the primary array control requirements with a small number of more complex shepherd satellites (*shepsats*), the large number of individual science satellites that make up the formation can be reduced in size and power or improved in capability without an increase in satellite mass. In addition to station-keeping large array formations, the proposed shepherd satellite concept can also be extended to the angular positioning of cooperative space telescope arrays and perhaps even to the in-situ shaping of flexible thin-film optical components for the future space-based telescope systems evaluated under a recent NIAC grant.[10]

The proposed shepherd satellite concept is based on the use of electromagnetic radiation forces to position and hold a large number of small, specialized spacecraft in a precise array. The concept derives from well-known optical scattering and gradient force techniques, which have been used to trap and manipulate microscopic objects using laser radiation. Although the presumed physical dimensions of the satellites will preclude the use of optical wavelengths, it is proposed that a technique similar to laser optical trapping can be used at millimeter or microwave frequencies more appropriate to larger object sizes.

Section 2.0 describes the physics of electromagnetic radiation forces trapping at microscopic scales, and discusses the primary assumptions used in the force analysis for the shepherd satellite concept. Section 3.0 outlines a set of mission applications that were evaluated during the Phase I project, ranging from drag make-up in low earth orbit to array station-keeping in geosynchronous, Lagrangian, and heliocentric Earth-trailing orbits. Section 4.0 provides a brief survey of microwave beam generation and steering techniques, and Section 5 concludes the report with a summary of the key Phase I results and suggested areas for further research.

2.0 ELECTROMAGNETIC RADIATION FORCES

During the past few decades, a number of experiments have demonstrated optical radiation force trapping of small dielectric and metallic particles using low power laser radiation.[27-36] A variety of smooth and irregularly shaped objects with diameters either equal to or larger than the optical wavelength (Mie particles) or significantly smaller than the incident optical wavelength (Rayleigh particles) have been successfully trapped, and the technique has become a standard tool for biological cell manipulation and micromachine fabrication.

Typical optical trapping experiments utilize a single-beam gradient force optical trap, also known as optical tweezers, to manipulate particles immersed in various types of liquid or gas media. In this approach, a laser beam is focused through a microscope objective to provide a radiation pressure force. The radiation pressure force consists of several components, including scattering, absorption, and gradient forces. Scattering and absorption forces arise due to the momentum transfer of scattered or absorbed photons, respectively. These forces are proportional to the difference between the light intensity (Poynting vectors) of the incident beam and the reflected or absorbed beams, and generally point along the direction of the incident beam. The gradient force is proportional to the gradient of the light intensity, and points toward regions of high intensity (typically a laser focal point). For stable trapping, the gradient force must exceed the scattering and absorption forces, as well as overcome other ancillary effects such as possible radiometric forces due to an asymmetric heating of the medium surrounding the particle. Three-dimensional single-beam gradient force traps have been successfully demonstrated for dielectric Mie and Rayleigh particles, and for small metallic Rayleigh particles.[27-29] Experimental 3-D single-beam traps have been less successful for metallic Mie particles, primarily due to the larger radiometric forces associated with the immersion medium.[30] Nevertheless, successful 2-D trapping of metallic Mie particles, as well as the simultaneous trapping of several particles in a linear array, has recently been reported.[31] In addition, the simultaneous trapping of several dielectric particles has recently been demonstrated using a Gaussian standing wave created by the optical interference of an incident and reflected laser beam.[32] In this experiment, a number of steep intensity gradients were created between the nodes and antinodes of the standing wave, providing several gradient force traps with axial separations equal to exactly half the laser wavelength.

A significant amount of theoretical analysis and numerical modeling has also been performed in an attempt to better understand the physics of optical trapping.[29,37-51] The two primary approaches used to simulate optical gradient forces acting on a particle are the electromagnetic wave approximation, used when particle dimensions are much smaller than the incident wavelength, and geometric or ray optics theory, used when particle dimensions are significantly larger than the incident wavelength. In the electromagnetic wave model, the incident electromagnetic radiation is decomposed into plane wave components using Fourier transforms, and the Maxwell stress tensor is then calculated to find the force acting on the particle. For particle sizes much smaller than the optical wavelength, the electromagnetic wave approach reduces to a dipole approximation in which particle interactions with the electromagnetic field are accurately modeled using standard electric dipole theory. When the particle dimensions are significantly larger than the incident optical wavelength, the electromagnetic wave approximation gives way to geometric optics theory. The geometric optics or ray model uses a vector sum of the rays reflected

and refracted from the particle to calculate the net force acting on the particle. The electromagnetic wave theory is accurate for particle dimensions several times smaller than the optical wavelength, while the geometric optics theory is accurate for particle dimensions roughly 10 times larger than the optical wavelength. In intermediate regimes, where the particle size is approximately the same as the incident wavelength, more intuitive models are employed, with varying degrees of success. To date, the most successful models in this intermediate size regime are restricted to spherical dielectric particles,[29] while the electro-magnetic and geometric optics models have been successfully used for a variety of particle shapes.

2.1 Radiation Force on Dielectric Rayleigh Particles

Harada and Asakura[38] calculate the radiation force for a spherical dielectric particle whose diameter is substantially smaller than the wavelength of the incident radiation. The incident beam is linearly polarized and is assumed to have a Gaussian distribution centered around a minimum beam radius of w_0. The polarization of the electric field is in the +x direction, the orthogonal magnetic field is in the +y direction, and the direction of propagation is in the +z direction. The dielectric particle is assumed to have radius *a* and dielectric constant ε_1, and is immersed in a medium with dielectric constant ε_2 and magnetic permeability μ_2. Further assuming a nonmagnetic medium, the magnetic permeability reduces to that of free space ($\mu_2 = \mu_0$). The dielectric constants are related to the dielectric constant of free space, ε_0, by the constitutive relations $\varepsilon_1 = \varepsilon_1 n_1^2$ and $\varepsilon_2 = \varepsilon_2 n_2^2$, where n_1 and n_2 are the index of refraction for the particle and medium, respectively.

The form of the electric field, polarized in the +x-direction, is given by:

$$\vec{E}(r) = \hat{x}E(r) = \hat{x}E_0 \left\{ \frac{ikw_0^2}{ikw_0^2 + 2z} \exp\left[-ikz\right] \right\} \left\{ \exp\left[-i \frac{2kz\left(x^2 + y^2\right)}{\left(kw_0^2\right)^2 + \left(2z\right)^2} \right] \right\} \left\{ \exp\left[-\frac{\left(kw_0\right)^2\left(x^2 + y^2\right)}{\left(kw_0^2\right)^2 + \left(2z\right)^2} \right] \right\} \quad (1)$$

where E_0 is the electric field strength at the center of the beam waist (x=y=z=0), k is the wave number ($2\pi/\lambda$), and λ is the wavelength of the incident radiation. The magnetic field component of the beam is:

$$\vec{H}(r) = \hat{z} \times \frac{\vec{E}(r)}{\sqrt{\mu_2 / \varepsilon_2}} \approx \hat{y} n_2 \varepsilon_0 c E(r) = \hat{y} H(r) \quad (2)$$

where *c* is the speed of light, given by $c = (\varepsilon_0 \mu_0)^{-1/2}$. The full time-dependent expressions for the electric and magnetic field vectors are then given by:

$$\begin{aligned} \vec{E}(r,t) &= \mathrm{Re}\left[\vec{E}(r)e^{i\omega t}\right] \\ \vec{H}(r,t) &= \mathrm{Re}\left[\vec{H}(r)e^{i\omega t}\right] \end{aligned} \quad (3)$$

where ω is the frequency of the electromagnetic radiation. The instantaneous energy flux contained in the beam, per unit area and per unit time in the direction of propagation, is given by the Poynting vector:

$$\vec{S}(r,t) \equiv \vec{E}(r,t) \times \vec{H}(r,t) = \tfrac{1}{2}\mathrm{Re}\left[\vec{E}(r) \times \vec{H}(r) e^{2i\omega t}\right] + \tfrac{1}{2}\mathrm{Re}\left[\vec{E}(r) \times \vec{H}(r)\right] \quad (4)$$

which is related to the beam intensity, **I**(r), through the relation:

$$\vec{I}(r) \equiv \left\langle \vec{S}(r,t) \right\rangle_t = \tfrac{1}{2}\,\mathrm{Re}\left[\vec{E}(r) \times \vec{H}^*(r)\right] = \hat{z}\frac{n_2 \varepsilon_0 c}{2}\left|E(r)\right|^2 = \hat{z} I(r) \tag{5}$$

where the function $\langle\rangle_t$ indicates a time-average is to be taken of the enclosed quantity. The magnitude of the beam intensity, I(r), is related to the beam power, *P*, by:

$$I(r) = \left(\frac{2P}{\pi w_0^2}\right)\frac{1}{1+\left(2\bar{z}\right)^2}\exp\left[-\frac{2\left(\bar{x}^2+\bar{y}^2\right)}{1+\left(2\bar{z}\right)^2}\right] \tag{6}$$

where the power is given by:

$$P = \tfrac{1}{4}\pi w_0^2 n_2 \varepsilon_0 c E_0^2 \tag{7}$$

For simplicity, the spatial coordinates in Equation 6 and future equations are normalized as follows:

$$\left(\bar{x},\bar{y},\bar{z}\right) = \left(x/w_0\,, y/w_0\,, z/kw_0^2\right) \tag{8}$$

Assuming the size of the dielectric particle is significantly smaller than the beam waist ($a<w_0$), the particle will act as a point dipole in the electric field, with an induced dipole moment given by:

$$\begin{aligned}\vec{p}(r,t) &= 4\pi\varepsilon_2 \frac{\varepsilon_1-\varepsilon_2}{\varepsilon_1+2\varepsilon_2} a^3 \vec{E}(r,t) \\ &= 4\pi\varepsilon_2 a^3\left(\frac{\varepsilon_1/\varepsilon_2-1}{\varepsilon_1/\varepsilon_2+2}\right)\vec{E}(r,t) \\ &= 4\pi\varepsilon_0 n_2^2 a^3\left(\frac{\kappa_r-1}{\kappa_r+2}\right)\vec{E}(r,t)\end{aligned} \tag{9}$$

where κ_r is the relative refractive index of the particle. With these definitions in place, the scattering and gradient forces expected to act on the particle can now be calculated.

2.1.1 Scattering Force

As the electric field oscillates in time, the induced dipole follows the electric field and acts as an oscillating electric dipole, radiating secondary waves in all directions. The scattered waves change the magnitude and direction of the energy flux of the incident beam, thus changing the momentum transferred to the particle by the beam. The force due to the scattering of the beam is given by:

$$\vec{F}_{scat}(r) = \frac{C_{pr}\left\langle \vec{S}(r,t)\right\rangle_t}{c/n_2} = \hat{z}\left(\frac{n_2}{c}\right)C_{pr} I(r) \tag{10}$$

where C_{pr} is the scattering cross section:

$$C_{pr} = \tfrac{8}{3}\pi(ka)^4 a^2\left(\frac{\kappa_r-1}{\kappa_r+2}\right)^2 \tag{11}$$

Substituting Equations 6 and 11 into Equation 10 yields the following form for the scattered radiation force acting on the particle:

$$\vec{F}_{scat}(r) = \hat{z}\frac{8n_2\pi(ka)^4a^2}{3c}\left(\frac{\kappa_r - 1}{\kappa_r + 2}\right)^2\left(\frac{2P}{\pi w_0^2}\right)\frac{1}{1+(2\bar{z})^2}\exp\left[-\frac{2(\bar{x}^2+\bar{y}^2)}{1+(2\bar{z})^2}\right] \tag{12}$$

The maximum force is found by setting x=y=0 in Equation 12 and finding the derivative with respect to z:

$$\vec{F}_{scat}(r)\Big|_{\max} = \hat{z}\frac{\partial F_{scat}(r)}{\partial\bar{z}}\Big|_{\bar{x}=\bar{y}=0} = 0 \tag{13}$$

Carrying out the derivative, the maximum scattering force is obtained for z=0, yielding:

$$\vec{F}_{scat}\Big|_{\max} = \hat{z}\frac{8n_2\pi(ka)^4a^2}{3c}\left(\frac{\kappa_r - 1}{\kappa_r + 2}\right)^2\left(\frac{2P}{\pi w_0^2}\right) \tag{14}$$

Equation 14 provides an analytic estimate of the maximum scattering force for a dielectric particle whose radius is smaller than the incident wavelength and beam radius ($a<\lambda<w_0$).

2.1.2 Gradient Force

The potential energy, *U*, of a dipole with moment $\vec{p}$ in an external electric field $\vec{E}$ is:[39]

$$U(r,t) = -\tfrac{1}{2}(\vec{p}\cdot\vec{E}) = -\tfrac{1}{2}pE\cos\vartheta \tag{15}$$

where θ is the angle between the dipole and the polarized electric field. For the case of an induced dipole, the dipole moment is parallel and in phase with the external electric field, hence θ = 0 and cos θ = 1. The force acting on the dipole is then given by the gradient in the potential energy:

$$\vec{F}_{grad}(r,t) = -\nabla U(r,t) \tag{16}$$

Substituting Equations 9 and 15 into Equation 16 yields:

$$\vec{F}_{grad}(r,t) = \tfrac{1}{2}\nabla(\vec{p}\cdot\vec{E})_{\vartheta=fixed} = \tfrac{1}{2}\nabla\left(4\pi\varepsilon_0 n_2^2 a^3\left(\frac{\kappa_r - 1}{\kappa_r + 2}\right)\vec{E}(r,t)\cdot\vec{E}(r,t)\right) = 4\pi\varepsilon_0 n_2^2 a^3\left(\frac{\kappa_r - 1}{\kappa_r + 2}\right)\tfrac{1}{2}\nabla E^2(r,t) \tag{17}$$

for the instantaneous gradient force exerted on the induced dipole by the external electromagnetic field. Taking the time average of Equation 17 provides an expression for the average gradient force exerted on the particle:

$$\vec{F}_{grad}(r) = \left\langle\vec{F}_{grad}(r,t)\right\rangle_t = 4\pi\varepsilon_0 n_2^2 a^3\left(\frac{\kappa_r - 1}{\kappa_r + 2}\right)\tfrac{1}{2}\nabla\left\langle E^2(r,t)\right\rangle_t \tag{18}$$

The time average of the electric field is given by:

$$\left\langle \vec{E}(r,t) \right\rangle_t = \tfrac{1}{2}\left|E(r)\right|^2 \tag{19}$$

and the expression for the average gradient force becomes:

$$\vec{F}_{grad}(r) = \pi\varepsilon_0 n_2^2 a^3 \left(\frac{\kappa_r - 1}{\kappa_r + 2}\right)\nabla\left|E^2(r)\right| \tag{20}$$

Using Equation 5, the gradient force can be expressed in terms of the average beam intensity, *I*:

$$\vec{F}_{grad}(r) = \frac{2\pi n_2 a^3}{c}\left(\frac{\kappa_r - 1}{\kappa_r + 2}\right)\nabla I(r) \tag{21}$$

Substituting Equation 6 for the intensity yields a useful form for the average gradient force in terms of beam power, shown below in component form:

$$\vec{F}_{grad,x} = -\hat{x}\frac{2\pi n_2 a^3}{c}\left(\frac{\kappa_r - 1}{\kappa_r + 2}\right)\left(\frac{4\bar{x}/w_0}{1+(2\bar{z})^2}\right)\left(\frac{P}{\pi w_0^2}\right)\left(\frac{1}{1+(2\bar{z})^2}\right)\exp\left[-\frac{2\left(\bar{x}^2+\bar{y}\right)}{1+(2\bar{z})^2}\right] \tag{22}$$

$$\vec{F}_{grad,y} = -\hat{y}\frac{2\pi n_2 a^3}{c}\left(\frac{\kappa_r - 1}{\kappa_r + 2}\right)\left(\frac{4\bar{y}/w_0}{1+(2\bar{z})^2}\right)\left(\frac{P}{\pi w_0^2}\right)\left(\frac{1}{1+(2\bar{z})^2}\right)\exp\left[-\frac{2\left(\bar{x}^2+\bar{y}\right)}{1+(2\bar{z})^2}\right] \tag{23}$$

$$\vec{F}_{grad,z} = -\hat{z}\frac{2\pi n_2 a^3}{c}\left(\frac{\kappa_r - 1}{\kappa_r + 2}\right)\left(\frac{8\bar{z}/\left(kw_0^2\right)}{1+(2\bar{z})^2}\right)\left(\frac{P}{\pi w_0^2}\right)\left(\frac{1}{1+(2\bar{z})^2}\right)\exp\left[-\frac{2\left(\bar{x}^2+\bar{y}\right)}{1+(2\bar{z})^2}\right] \tag{24}$$

where again the normalized position coordinates are given by Equation 8. The maximum gradient force along the beam axis is found by setting x=y=0 in Equation 24 (the particle is located at the center of the beam waist), then setting the z-derivative of the resulting equation equal to zero:

$$\vec{F}_{grad}(0,0,\bar{z}) = -\frac{32 n_2 a^3 \bar{z} P}{ckw_0^4}\left(\frac{\kappa_r - 1}{\kappa_r + 2}\right)\left(\frac{1}{1+(2\bar{z})^2}\right)^2 \tag{25}$$

$$\left.\frac{\partial F_{grad,z}(0,0,\bar{z})}{\partial \bar{z}}\right|_{\max} = 0 \tag{26}$$

The result indicates that the maximum axial force is achieved when $\bar{z} = \frac{1}{(2\sqrt{3})}$, or in terms of the dimensional axial coordinate, $z = \frac{kw}{2\sqrt{3}}$. Substituting this value into Equation 25 yields an expression for the maximum gradient force in the axial (beam) direction:

$$\left.\vec{F}_{grad,z}\right|_{\max} = -\hat{z}\left\{5.2\frac{n_2 a^3 P}{ckw_0^4}\left(\frac{\kappa_r - 1}{\kappa_r + 2}\right)\right\} \tag{27}$$

The negative sign in Equation 27 indicates the gradient force acts back along the direction of beam propagation, in the direction of the beam focal point.

Similar exercises can be performed to find the maximum transverse gradient forces acting on the particle in the x and y directions. These forces provide restoring forces that pull the particle back toward the beam axis, and are given by:

$$\vec{F}_{grad,x} = 2.43\frac{n_2 a^3 P}{c w_0^3}\left(\frac{\kappa_r - 1}{\kappa_r + 2}\right)\hat{x} \tag{28}$$

$$\vec{F}_{grad,y} = 2.43\frac{n_2 a^3 P}{c w_0^3}\left(\frac{\kappa_r - 1}{\kappa_r + 2}\right)\hat{y} \tag{29}$$

Together with the axial gradient force, these transverse gradient forces provide a stable electromagnetic trap that holds the dielectric particle in place. Typical force levels predicted by Equations 27-29 for small dielectric particles are in the range of 0.01-pN/mW to 1-pN/mW, or approximately 10^{-11}N/W to 10^{-9} N/W, and typically agree within a factor of a few with experimental results.[32-34,38]

2.2 Radiation Force on Metallic Rayleigh Particles

Analytic models for the scattering and gradient forces acting on small metallic particles are essentially identical to models for dielectric Rayleigh particles, with the exception that the polarization of the particle depends on the skin depth of the metal.[35] As such, Equation 14 for the scattering force and Equations 27-29 for the gradient forces are still valid as long as the skin depth, δ, satisfies the condition:

$$\delta = \frac{\lambda}{2\pi k} >> a \tag{30}$$

where a is the particle radius. Comparisons with experiment[35,36] yield an approximate force per power ratio in the range of 10^{-11}-N/W to 10^{-9} N/W, similar to the range of forces obtained for dielectric Rayleigh particle experiments.

2.3 Radiation Force on Dielectric Mie Particles

Moving to particle sizes larger than the wavelength of the incident electromagnetic radiation shifts the analysis from a purely electromagnetic approximation to a regime where simpler ray-optics models can be employed. A simple yet accurate model by Wright, Sonek and Berns[40] relates the scattering and gradient forces to a set of non-dimensional trapping efficiencies, Q_s and Q_g for a single incident beam:

$$F_s = \frac{n_1 Q_s P}{c} \tag{31}$$

$$F_g = \frac{n_1 Q_g P}{c} \tag{32}$$

where n_1 is the refractive index of the medium surrounding the particle, P is the incident beam power, c is the speed of light in the medium. The non-dimensional efficiency parameters Q_s and Q_g are calculated by analyzing the momentum transferred to a spherical dielectric particle by an incident beam, part of which is reflected and part of which is transmitted through the particle surface:

$$p_s = \left\{1 + R\cos(2\vartheta_1) - \frac{T^2\left[\cos 2(\vartheta_1 - \vartheta_2) + R\cos(2\vartheta_1)\right]}{1 + R^2 + 2R\cos\vartheta_2}\right\} p_i = Q_s p_i \tag{33}$$

$$p_g = \left\{R\sin(2\vartheta_1) - \frac{T^2\left[\sin 2(\vartheta_1 - \vartheta_2) + R\sin(2\vartheta_1)\right]}{1 + R^2 + 2R\cos\vartheta_2}\right\} p_i = Q_g p_i \tag{34}$$

In Equations 33 and 34, p_i, p_s, and p_g represent the incident momentum, scattered momentum (parallel to incident beam), and gradient momentum (transverse to the incident ray); R and T are the Fresnel reflection and transmission coefficients, θ_1 is the incident angle, and θ_2 is the refraction angle. Based on the ray model, Wright, Sonek and Berns develop an algorithm to perform a vector summation of the contribution of all rays with convergence angles from zero to a given maximum convergence angle; similar algorithms are used to calculate both axial and transverse forces. The results of their calculations for silica dielectric particles immersed in a water medium agree fairly well with experiments, and indicate axial trapping efficiencies on the order of 0.01 to 0.1 depending on particle size and axial location of the beam focus. Transverse trapping force efficiencies are slightly higher, with Q values ranging from 0.1 to 0.4, again depending on model assumptions. The overall result of their analysis indicates that trapping forces for dielectric Mie particles are on the order of 1-5 pN/mW, or around 10^{-9} N/W, in approximate agreement with the magnitude of trapping forces imposed on dielectric and metallic Rayleigh particles.

The results of Wright, Sonek and Berns agree with the predictions of a slightly more complex geometric optics model developed by Gussgard, Lindmo, and Brevik.[41] In the latter model, the energy momentum tensor is used to analyze the force exerted on a spherical dielectric Mie particle centered on the axis of the incident beam. The force levels predicted by Gussgard, Lindmo and Brevik under conditions similar to the model of Wright, Sonek and Berns are approximately the same as the former model, indicating gradient forces on the order of 10^{-9} N/W.

2.4 Radiation Force on Metallic Mie Particles

Extending the optical models from dielectric to metallic Mie particles introduces some additional complications due to the skin depth of the particle surface, which is typically only several nanometers and hence is significantly smaller than the incident optical wavelength. As such, the constraint posed by Equation 30 does not hold, and the analysis of the trapping force no longer includes the effects of multiple reflections by rays transmitted through the particle surface. A model that takes these effects into account has been developed by Ke and Gu,[42] who find that momentum change of the particle is primarily due to the reflection of the incident beam at the particle surface. The scattering and gradient forces caused by a single ray incident on the particle surface are then given by:

$$F_s = \frac{n_1 P}{c}(1 + R\cos 2\vartheta) \tag{35}$$

$$F_g = \frac{n_1 R P}{c}\sin 2\vartheta \tag{36}$$

where again R is the reflectance of light at the particle surface, n_1 is the refractive index of the medium, P is the incident beam power, c is the speed of light, and θ is the angle of incidence of the ray with respect to the surface normal. Note that the scattering force always acts along the direction of the beam, while the gradient force acts in the direction of the beam focus; if the gradient force is upstream of the particle, the scattering and gradient forces work in opposite directions and the gradient force must be sufficiently large to overcome the scattering force and provide stable trapping. The model integrates the scattering and

trapping forces over all angles of convergence, and the results are used to define axial and transverse trapping efficiencies, which are given by the general expression:

$$Q = \frac{Fc}{n_1 P} \tag{37}$$

The calculated values for the (optical) axial trapping efficiency, Q_a, for a spherical metallic particle range from an approximate value of 2 for a gold sphere to 3 for a silver sphere; transverse trapping efficiencies for these materials range from 0.3 to 1.25, respectively. The model predictions were compared to experimental results for laser beams focused by lenses of given numerical apertures, in which case the values of the axial and transverse trapping efficiencies were approximately 0.6 and 0.1, respectively. The results were in fair agreement with experiment, predicting axial and transverse forces that once again are on the order of a few pN per mW of incident laser power. An interesting observation, both from the model and experimental results, is that unlike the case of dielectric particles, metallic Mie particles are always pushed along the direction of the incident beam due to the reflective nature of the radiation force.

2.5 Summary of Single Beam Force Models

Radiation pressure forces are typically composed of scattering, absorption, and gradient force components. Scattering forces are due to the momentum of incident beam photons scattered from the object surface, while absorption forces arise from the momentum transferred by beam photons absorbed by the object. Both of these forces are proportional to the intensity of the incident beam, and act in the direction of beam propagation. Gradient forces are generated by the interaction of a focused electromagnetic wave with the dipole field it induces in an electrically polarizable object; the resulting force on the electric dipole is proportional to the gradient in beam intensity, in the direction of the focus of the incident beam. In most models the absorption forces are presumed to be negligible with respect to the scattering and gradient forces, and are ignored. Based on the models presented above for single beam optical traps, typical radiation force values are expected to range from roughly 10^{-11} N/W to around 10^{-9} N/W. It is anticipated that these same force levels can be achieved in the shepherd satellite concept, where the larger satellite dimensions are offset by the longer electromagnetic wavelengths of the incident beams. Because most array satellites are expected to greatly exceed the wavelength of the microwave beams envisioned for use in the shepsat concept, the force approximations for Mie particles (Sections 2.3-2.4) will be used to analyze potential mission applications in Section 3.0 below.

3.0 SHEPHERD SATELLITE MISSION APPLICATIONS

Based on the results of Section 2.0, the average radiation force acting on a Mie particle is approximately 10^{-9} N/W. It is anticipated that this same force level can be achieved in the shepherd satellite concept, where an array satellite can be effectively modeled as a Mie particle with dimensions significantly larger than the incident microwave wavelength. The following sections outline a variety of potential mission applications for which the shepherd satellite concept might be employed, describing both the benefits and limitations for each application. A brief summary of the reviewed mission applications is presented in Section 3.7.

3.1 Low Earth Orbit (LEO)

The dominant orbital perturbation in low earth orbit is due to atmospheric drag, a non-conservative force that progressively removes energy from the satellite and leads to a decrease in orbital altitude. To better understand the magnitude of the forces involved, two computer programs were written to parametrically

evaluate the minimum and maximum drag forces for a variety of satellite cross sectional areas and circular orbit altitudes. Cross sectional areas were chosen from 0.1-m^2 to 2-m^2 to provide flexibility in the potential orientation of satellite bodies to the direction of motion. Standard models were used to estimate maximum and minimum atmospheric mass densities from 200-km to 1000-km, and drag coefficients ranging from 2 to 4 were used to encompass the full range of possible drag values. The first computer program (Appendix A) employs user-input for satellite mass, cross-sectional area, and orbital radius to calculate minimum and maximum drag forces. The second code (Appendix B) performs a parametric analysis over the full range of values listed above and stores the data in text format for later evaluation. The sections below outline the basic calculations included in each code and discuss some preliminary results for the drag forces to be expected on typical small satellites in low earth orbit.

3.1.1 Drag Formulas

The drag, F_D, on a spacecraft in low earth orbit is given by the formula:

$$F_D = \frac{1}{2} m \rho V^2 B^{-1} \tag{38}$$

where m is the spacecraft mass, ρ is the atmospheric mass density at a given orbital radius, V is the orbital velocity, and B is the ballistic coefficient, given by:

$$B = \frac{m}{C_D A} \tag{39}$$

In Equation 2, A is the spacecraft cross sectional area in the direction of motion, and C_D is an empirical drag coefficient, with value typically ranging from 2 to 4. The units for the ballistic coefficient, B, are kg-m^{-2}. Note that substituting Equation 2 into Equation 1 eliminates the dependence of the frag force on spacecraft mass.

For this preliminary analysis, the orbital velocity, V, is calculated for simple circular orbits using the formula:

$$V = \sqrt{\frac{GM}{R}} \tag{40}$$

where G is the universal gravitational constant, 6.6726x10-11 N-m^2/kg^2, M is the mass of the earth, 5.976x10^{24} kg, and R is the orbital radius with respect to the earth's center.

The atmospheric mass density can be estimated using the standard COSPAR International Reference Atmosphere model for orbits up to approximately 400-km,[52] and from the MSIS thermospheric model for higher orbits.[53] The COSPAR model is presented in Figure 1, while the maximum and minimum atmospheric mass density values predicted by the MSIS model are displayed in Figure 2.

3.1.2 Code Validation

To test the simulations, drag predictions were made for the "Three-Corner Cube" or 3CS satellite, a joint venture between Arizona State University, the University of Colorado at Boulder, and New Mexico State University. The predicted drag forces published for the 3CS satellite orbiting at an altitude of 350-km range from 0.04-mN to 0.14-mN, depending on the value of the drag coefficient used to evaluate the ballistic coefficient in Equation 2. Using similar values for the spacecraft mass (15-kg) and cross sectional

area (0.14-m^2), the code listed in Appendix A predicts minimum and maximum drag forces of 0.04-mN and 0.16-mN, respectively, in good agreement with the published values.

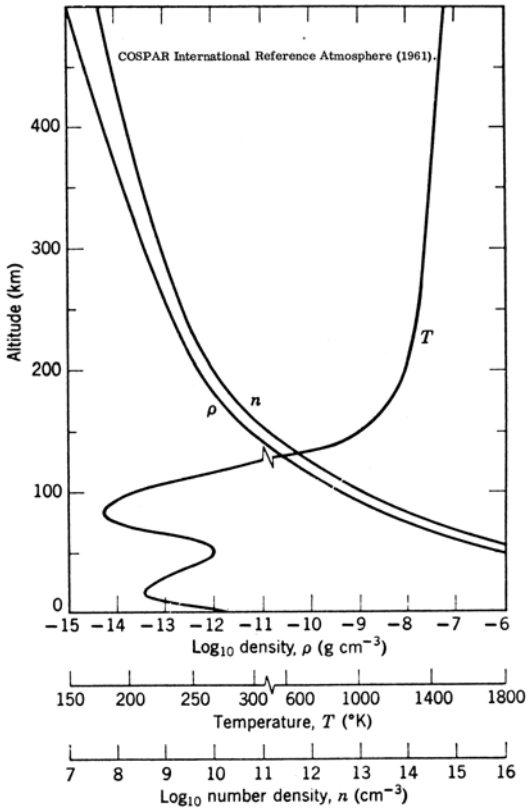

Figure 1. COSPAR atmospheric density model.[52]

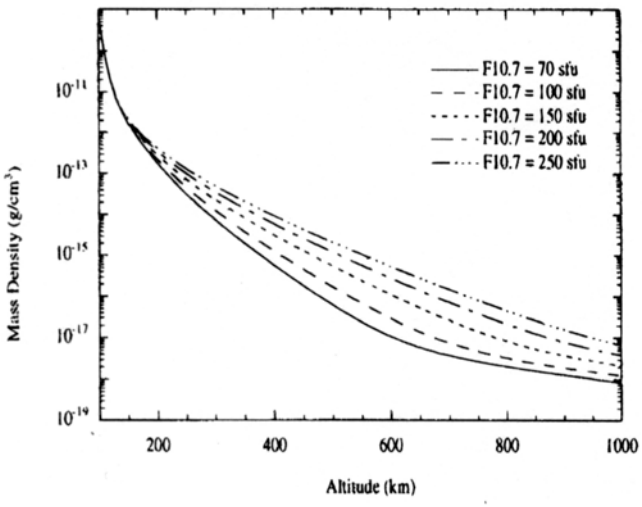

Figure 2. MSIS atmospheric density model.[54]

3.1.3 Drag Force Corrections in LEO

Figure 3 plots typical drag forces encountered in LEO for a range of spacecraft cross sections, at altitudes ranging from 200 km to 1000 km and atmospheric densities corresponding to minimum and maximum solar wind conditions. Overlaid on the plot is a horizontal line depicting the 10^{-5} N force level that can be generated using a modest 10-kW microwave beam. Note the vertical axis is in units of mN (10^{-3} N).

Figure 3 indicates that for the worst-case solar models, the predicted radiation force of 10^{-2} mN generated by a 10-kW microwave beam can overcome atmospheric drag for a wide range of microsatellite cross sectional areas at orbital altitudes above roughly 800-km. Because of the relative uncertainty in the predicted radiation force and because the cross sectional areas of the microsats constituting a potential formation-flying array have not yet been determined, Figure 3 is at best a preliminary guide to viable regimes for shepsat operation in LEO. If the actual radiation forces generated by a 10-kW beam are indeed equal to the predicted value of 10^{-2} mN, then the shepsat concept can counter atmospheric drag for small (0.1 m^2) microsats at orbital altitudes as low as 500-km, and can sustain the orbits of larger microsats above 800-km. While it is anticipated that numerical modeling may provide better estimates of the scattering and gradient radiation forces provided by the shepherd satellites, the uncertainties inherent is such models indicate that an experimental approach may be required to ascertain more accurate radiation force values and their ability to compensate drag perturbations in low earth orbit.

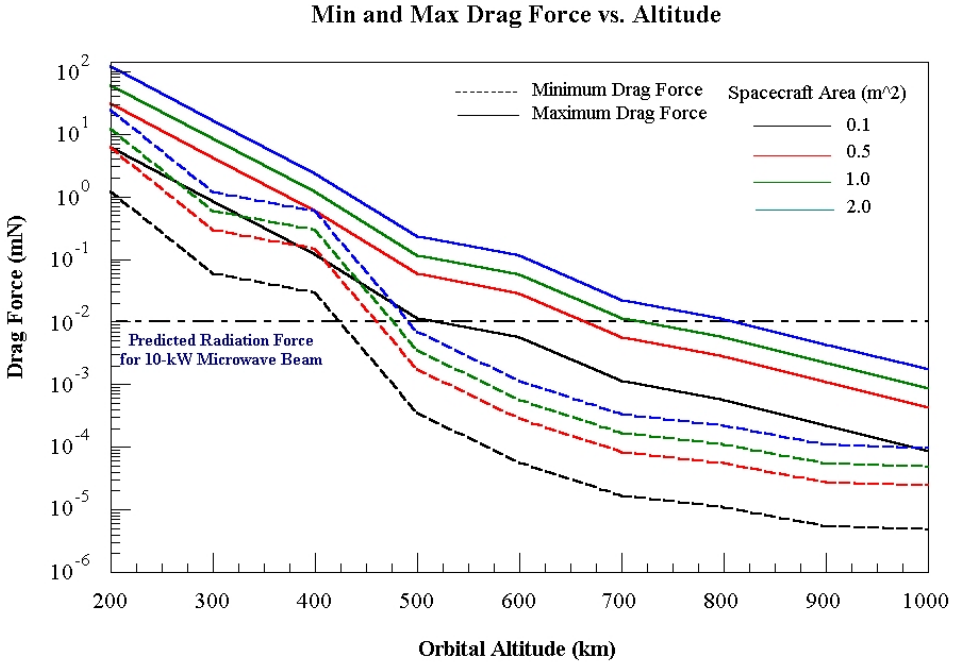

Figure 3. Drag force vs. orbital altitude.

Assuming the radiation forces are sufficient to overcome atmospheric drag, the question arises as to how often the array must be illuminated to keep the satellites in formation. If the radiation force is just equal to the drag force, the microsat will have to be kept under constant illumination by the shepsat to provide continual cancellation of the drag force. Clearly, if one 10-kW shepsat is required to keep one microsat in place in orbit, the concept is not feasible. What is required instead is a radiation force significantly larger than the drag force, such that the shepsat illuminates a given microsat for a portion of the beam duty cycle, allowing the beam to illuminate a number of microsats in sequence. Ideally, the radiation force would be at least equal to the drag force multiplied by the number of microsats in the array. This would allow a single shepherd satellite to provide a sufficient restoring force to each of the microsats.

To evaluate the required restoring force, a simple program was written to determine the microsatellite drift due to the competing effects of atmospheric drag and radiation forces (Appendix C). It is assumed that the radiation force is directed exactly opposite to the drag force, and the displacement along the direction of the orbit is sufficiently small that simple linear force equations can be used. The model solves the general force equation,

$$\overline{F}_{net} = \overline{F}_{rad} - \overline{F}_{drag} \tag{41}$$

from which the microsatellite drift, Δx, can be determined as a function of time:

$$\Delta x = \tfrac{1}{2} \frac{F_{net}}{m} t^2 \tag{42}$$

where m is the microsat mass. During illumination by the 10-kW beam, the radiation force F_{rad} overcomes the drag force F_{drag} to move the satellite slightly ahead in its orbit; when the illumination is turned off, the drag force moves the microsat slightly back in its orbit. By specifying a tolerable drift distance, Δx, the required beam illumination time and permissible drift time (without illumination) can be determined.

As an example, assume a large 50-kg microsat has a cross-sectional area of 1-m^2 and is in an orbital altitude of 1000-km. From Figure 3, the approximate maximum drag force on the satellite is 10^{-3} mN. Further assume that the radiation force provided by the 10-kW shepsat is 10^{-2} mN, and the maximum allowed satellite drift in the direction of its orbit is ± 1cm (0.01 m). The results of the force simulation are shown in Figure 4 below. To keep the microsat positioned to within ± 1cm requires the shepsat to illuminate the microsat for a period of approximately 0.67 hours. The microsat is then allowed to drift due to drag forces for a period of around 5.72 hours before it is once again illuminated by the shepsat. The competition between the drag and restoring forces keep the microsat to within ± 1cm of its required orbit location. Because the shepsat only has to illuminate the microsat for 0.67 hours out of every 6.39 hours, a total of 9 microsats can be sequentially illuminated by a single 10-kW shepherd satellite. Increasing the power of the beam would allow a shorter illumination period to provide the same restoring force, allowing more microsatellites to be illuminated by a single shepherd satellite. Conversely, a microsatellite with smaller mass would require less illumination time to restore it to its position in the array (Equation 42), indicating that a larger number of smaller microsatellites could be held in position by a single shepsat. Based on this preliminary analysis, it appears at least feasible that the proposed concept can generate sufficient restoring forces to counter even the worst-case atmospheric drag at altitudes exceeding 1000-km. Below that altitude, the restoring forces will probably not be sufficient to allow the sequential illumination of several microsats, making the concept potentially less attractive for the drag compensation of large cross-sectional area satellites.

A potential application for the shepsat concept in LEO is to maintain the spacing of a linear (equal inclination and altitude) array of small observation satellites focused toward either earth or space. Such a linear array of microsatellites might be used for hyperspectral Earth imaging applications, long baseline observations, or interferometry of astrophysical sources. A single shepsat flying ahead or behind the array at the same orbital altitude would have its line of sight blocked and would not be able to sequentially illuminate all of the satellites in the formation. As such, the shepsat would have to fly at a higher or lower altitude than the microsatellite array, while either leading (for gradient forces) or trailing (for scattering forces) the formation. However, in addition to providing the desired component of force along the direction of motion, this location would introduce a force component perpendicular to the orbital direction that would change the orbital altitude of the microsatellite under illumination. As such, two shepsats are apparently required for a linear formation flying array; one to fly above the array, and one to fly below the

array. Each shepherd satellite would simultaneously illuminate a given microsatellite, such that the perpendicular force components would cancel. Because the beam is no longer head-on, the force component along the direction of motion would be reduced by the cosine of the angle between the incident beam and the microsatellite surface; however, the angle required for a useful line of sight will generally be small, and because two shepsat beams will simultaneously illuminate each microsatellite, the cosine loss term is not anticipated to pose a serious problem. In some instances, out-of-plane forces may actually be desired to compensate for a given orbital perturbation or to re-arrange the formation, in which case the beam intensities can be adjusted to provide the required net force components along and perpendicular to the direction of motion.

As previously noted, the advantage to using an array of smaller satellites is in the ease and economy of replacement should one of the sensor satellites malfunction; that microsatellite can be deorbited from the array, and a replacement quickly launched to fill its place. This contrasts with the complex and costly task of launching a single, large sensor platform, in which the failure of one component could jeopardize the success of the entire mission. As an added benefit, the use of shepsats to provide drag compensation for the linear array mitigates potential problems that might otherwise arise from propellant contamination by individual microsatellite thrusters, keeping the observation sensors in pristine condition.

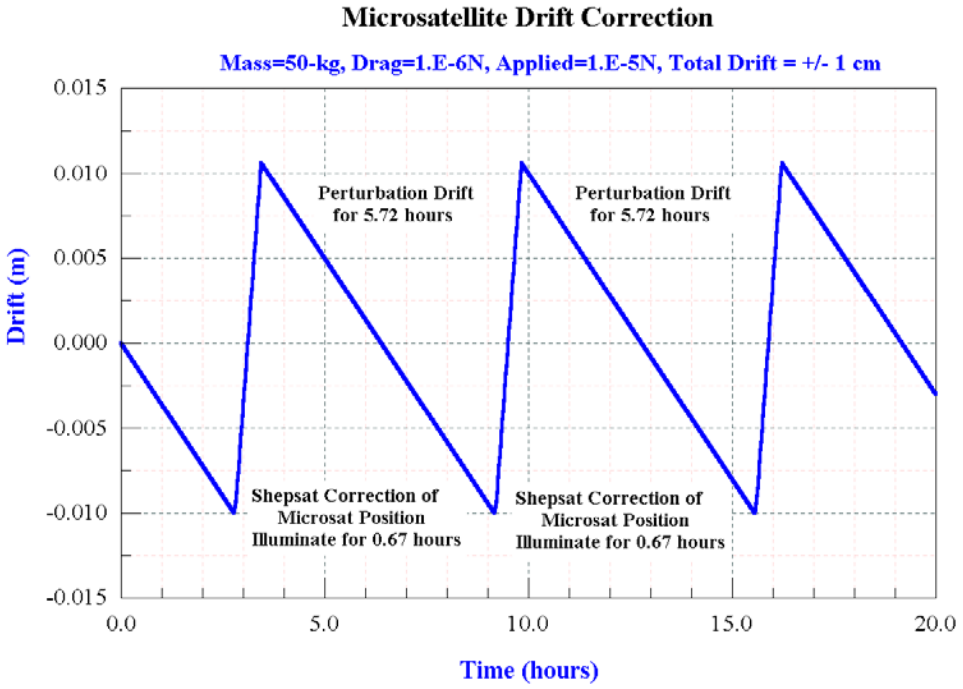

Figure 4. Drag compensation for a 50-kg, 1-m^2 microsatellite in a 1000-km orbit.

3.1.4 Other Applications in LEO

In instances where the radiation forces are unable to overcome drag in LEO, shepsats can still play a role in array guidance, navigation, and communication. In this capacity, the microsats would require a propulsion source to make up for drag and other orbital perturbations in low earth orbit. However, unlike current formation flying concepts in which all guidance and communication is provided by ground stations, these functions are instead performed using a single shepsat flying in formation with the microsatellite array. A focused microwave beam provided by the shepsat is used to provide an intensity beacon or orbital "mark" for the microsats to follow; a single shepsat can be used to sequentially

illuminate the precise orbital location that a microsatellite should occupy, and the microsatellite can use simple sensors and on-board propulsion to adjust its position accordingly.

In practice, each microsatellite can be fitted with an electromagnetic intensity gradient sensor positioned on a small boom in front of the satellite, pointing along the direction of the orbit. The array formation pattern is presumably known in advance, allowing the shepherd satellite to precisely and repeatedly mark the desired pattern with a scanning, focused microwave beam. A simple autonomous program on each microsatellite can be used to control the microsat propulsion system to maintain the intensity sensor at the point of maximum intensity. Rather than having ground stations trying to keep track of and adjust the position of several microsatellites, or having each microsatellite sense and adjust their position according to the location of other microsatellites in the array, the microsats need only adjust their positions to stay at a point of maximum intensity generated by the shepherd satellite. The concept provides a stable, on-orbit reference frame for each microsatellite in the array, greatly simplifying the guidance, command and control requirements. In addition, the spot locations can be changed to alter the formation pattern; each microsatellite will follow its designated intensity spot to a new location in the array. This technique can also simplify on-orbit positioning of new or replacement array elements; each new microsatellite can be guided into position by following an intensity spot provided by the shepherd satellite flying on the outskirts of the array. While this scenario requires that the microsatellites retain propulsion capabilities, the use of intensity beacons to provide an on-orbit reference frame potentially simplifies the array guidance and control requirements. Ground stations need only keep track of and adjust the shepherd satellite orbit location; the shepherd satellite in turn sets the locations of the more numerous microsatellites using the described intensity reference matrix. As an added bonus, rather than the ground having to communicate with each individual microsatellite, the information gathered by the microsats can be relayed to the more powerful shepsat for collection and communication to the ground.

3.2 Medium Earth Orbit (MEO)

The same arguments listed in favor of the shepsat concept for LEO apply equally well to missions in MEO. Such missions might include repeat-track ground or ocean monitoring for earth and environmental science applications, battlefield intelligence or surveillance missions using high resolution distributed arrays, and similar classes of missions. Although atmospheric drag forces are considerably reduced in MEO, other orbital perturbations gain significance. These additional perturbations include effects on the satellite orbits due to the oblateness of the earth, earth triaxiality, sun-moon perturbations, and, at sufficiently high orbits, radiation pressure from the sun. As discussed above, at altitudes above 1000-km a 10-kW microwave beam can provide sufficient radiation force to overcome atmospheric drag; the other perturbations are smaller in magnitude, and it is anticipated that radiation forces can also be used to overcome these perturbations and hold the array in formation. With the exception of atmospheric drag, these same secondary perturbations also appear in geosynchronous orbits, hence they will be discussed in more detail in the following section.

3.3 Geosynchronous Earth Orbit (GEO)

A useful review of the perturbations encountered by a satellite in geosynchronous orbit is provided by Lovell and O'Malley,[55] the salient features of which are discussed below.

3.3.1 North-South perturbations due to the Sun and Moon

If left uncorrected, the sun and moon cause the orbit inclination to increase sinusoidally to a peak of 14.7^{o} over a 26.5-year period, then decrease to zero after 53 years. The growth in inclination over the first 5-year period is nearly constant at 0.85^{o}/year. The change in inclination causes an out-of-plane (north-

south) change in the orbit, and the satellite must thrust normal to the orbital plane to provide north-south station keeping.

The time rate of change of the inclination, *i*, provided by an acceleration, *W*, normal to the orbital plane is given by:[39]

$$\frac{di}{dt} = \frac{r\cos\varphi}{na^2\sqrt{1-e^2}}W \tag{43}$$

where *r* is the orbital radius, φ is the angle from the ascending node to the instantaneous position of the satellite, *n* is the orbital angular velocity, *a* is the orbit semi-major axis, *e* is the orbit eccentricity. Retaining only first-order terms in the eccentricity, Equation 43 can be more simply written as:

$$\frac{di}{dt} = \frac{\cos\varphi}{V}W \tag{44}$$

where V = 3075 m/s is the nominal satellite orbital velocity in GEO. Substituting the yearly change in inclination into Equation 4 yields:

$$W = \left(\frac{0.85^0}{1-\text{year}}\right)\left(\frac{1-\text{year}}{3.156\times10^7\,\text{sec}}\right)\left(\frac{2\pi\text{rad}}{360^o}\right)\left(\frac{3075\text{m/s}}{\cos\varphi}\right) = \left(\frac{1.45\times10^{-6}}{\cos\varphi}\right)\text{m/s}^2 \tag{45}$$

For a nearly equatorial geosynchronous orbit, the required acceleration normal to the orbital plane is thus around $1.45\text{x}10^{-6}$ m/s^2. A general relation between the beam power required for inclination compensation and the microsatellite mass can be derived using Equation 45. Assuming an upper bound of 10^{-9} N/W for the radiation force provided by a beam of power P, the radiation force can be equated to the required north-south station keeping force to yield:

$$P(W)\left(10^{-9}\,\frac{N}{W}\right) \geq M\left(\frac{1.45\times10^{-6}}{\cos\varphi}\right) \tag{46}$$

where M is the microsatellite mass in kg. Rearranging Equation 46, the power required to compensate for inclination perturbations is then given by:

$$P(W)\cos\varphi \geq (1.45\times10^3)M \tag{47}$$

The required power versus satellite mass is plotted in Figure 5 on the following page. As shown in the figure, a 10-kW beam can provide sufficient force to hold a 7-kg, nearly equatorial ($\cos\varphi \approx 1$) satellite in place against perturbations in inclination. However, this requires continuous illumination of the satellite by the 10-kW beam; if more than one satellite is to be illuminated, the beam power has to be increased in proportion. For example, to provide north-south station keeping of a 10-kg science satellite, the required beam power is approximately 14.5 kW. If a single shepsat is required to hold 5 micro-satellites in place, the total required beam power is approximately 72.5 kW. This power can be split among 5 beams independently projected by the shepsat, or a single beam can be scanned continuously between the microsatellites to provide the required station keeping forces. The total required power, while high, is not unreasonable for current solar array power systems. Nevertheless, station-keeping these perturbations in inclination appears most promising for small (<10-kg) microsatellite masses.

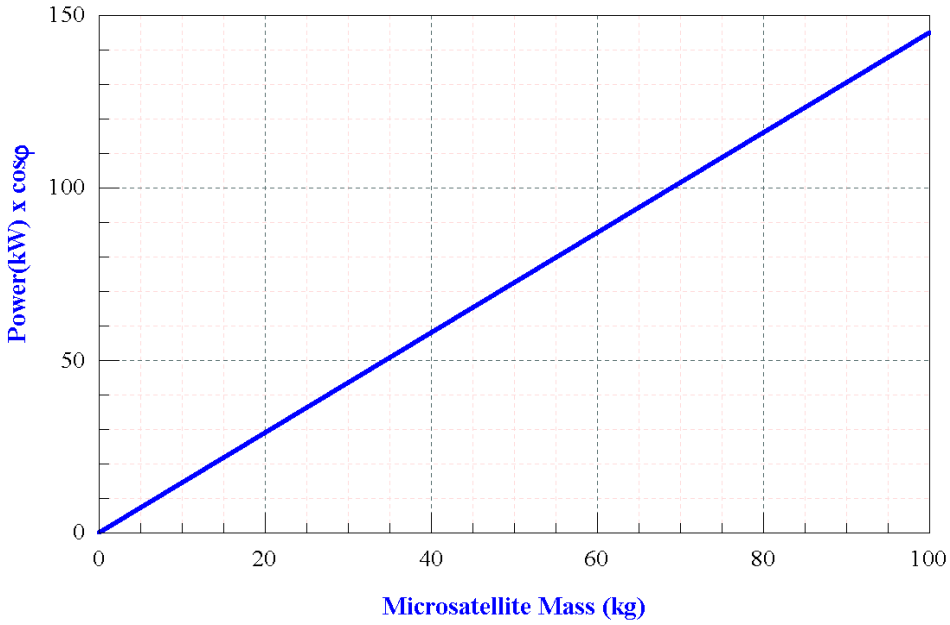

Figure 5. Required beam power vs. microsatellite mass for GEO north-south station keeping.

3.3.2 East-West Perturbations due to Solar Radiation Pressure

The effect of solar pressure impinging on a satellite is to change the orbital eccentricity and the orientation of the apsidal line. The perturbing acceleration, Δa, on a satellite of mass M and surface area A is given by:

$$\Delta a = S(1+\sigma)\frac{A}{M} \tag{48}$$

where S is the solar constant at 1-AU, $4.5\text{x}10^{-6}$ kg/(m-s^2), and σ is the average reflectivity of the satellite. Assuming a microsatellite mass of 10-kg, a cross-sectional area of 1-m^2, and an average reflectivity of 0.5 yields an in-pane perturbation due to solar radiation pressure of approximately $6.8\text{x}10^{-7}$ m/s^2. To counter this perturbation, an acceleration of at least this magnitude must be applied in a direction opposite to the direction of the incident solar radiation. As discussed above, the predicted radiation force on a microsatellite caused by a focused 10-kW beam is approximately 10^{-5} N; the acceleration produced by the beam on a 10-kg microsatellite is thus around 10^{-6} m/s^2, which exceeds the predicted acceleration caused by the incident solar radiation.

Based on Equation 48, the solar radiation force is given by $F_s = S(1+\sigma)A$, which provides a constraint on the satellite dimension (A) and reflectivity (σ) if the restoring force provided by the shepsat microwave beam is to exceed the perturbing solar radiation force:

$$(1+\sigma)A < 2.2\text{m}^2 \tag{49}$$

Equation 49 can be easily satisfied for reasonable microsatellite cross sectional areas and reflectivities, and the proposed concept should thus be able to correct in-plane perturbations due to solar radiation pressure.

3.3.3 East-West Perturbations Caused by Earth Triaxiality

The Earth's equatorial cross section is approximately elliptical, with an ellipticity of $6|J_2^{(2)}|$, where $J_2^{(2)}$ is equal to $-1.816\text{x}10^{-6}$. The minor axis of the ellipse passes through approximately 75° east longitude and 105° west longitude, which are stable points; a satellite placed at either of these longitudes will remain there, neglecting the other perturbations outlined above. If the satellite is positioned at any other longitude, it will tend to drift toward and oscillate about the nearest equilibrium point. The yearly change in velocity due to this perturbation is given by:[55]

$$\Delta V_t\left(\tfrac{m}{s}/\,yr\right) = 1.75\left|\sin(2\gamma_0)\right| \tag{50}$$

where γ_o is the desired spacecraft longitude. The maximum value of this east-west perturbation, corresponding to a longitude of 45° or 135°, is thus on the order of 1.75 m/s per year. The radiation force provided by a 10-kW beam is on the order of 10^{-5} N, which provides an acceleration of $2\text{x}10^{-7}$ m/s^2 to a 50-kg microsatellite. The required illumination period to make up a velocity change of 1.75 m/s is $8.75\text{x}10^6$ seconds, or approximately 0.277 years. Hence in one year, a single 10-kW beam can illuminate roughly four 50-kg satellites to maintain their orbit against the maximum triaxial perturbation; for smaller satellite masses, lower triaxial accelerations, or higher beam powers, more microsatellites can be illuminated in sequence by a single microwave beam to hold the formation against this orbital perturbation. Rearranging Equation 50 and equating the acceleration for a given satellite mass, M, to the radiation force of 10^{-9} N/W provided by a beam of power, P, yields:

$$(10^{-9}\,\tfrac{N}{W})P(W) \geq M(1.75\,\tfrac{m}{s}/\,year)(yr/3.156\times10^7 s)\left|\sin(2\gamma_0)\right| \tag{51}$$

which can be solved for the required beam power as a function of satellite mass and desired longitude:

$$P(W) \geq 55.45\times M\times\left|\sin(2\gamma_0)\right| \tag{52}$$

where M is the microsatellite mass in kg and γ_o is the desired longitude. This relation is shown in Figure 6 below. As an example example, if a 10-kg microsatellite is to be held at a desired longitude of 15°, the required beam power is approximately 190 W; to hold 10 microsatellites in place against triaxial orbit perturbations would require a total power of only 1.9-kW. At longitudes of 0°, 90°, and 180°, the triaxial perturbation falls to zero and no correction is required.

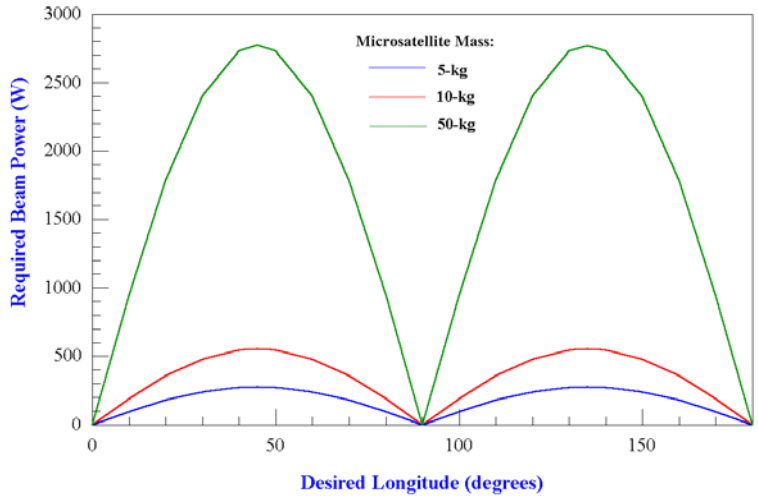

Figure 6. Beam power needed to correct orbit perturbations due to Earth's triaxiality.

3.4 Lagrangian and Other Orbit Applications

For astronomical observations, significant advantages in satellite station-keeping may be achieved by positioning the formation-flying array in a stable Lagrangian orbit or into a heliocentric earth-trailing orbit. As shown in Figure 7, for a planet moving around the Sun, there are five Lagrangian points in space at which a much smaller body (such as a satellite) will remain in a stable orbit with respect to the planet. The first Lagrange point (L1) is at the position in the planet's orbit that is diametrically opposite to that of the planet; the second and third Lagrange points (L2 and L3) are on a line between the Sun and planet, with L2 between the Sun and planet and L3 lying outside the orbit of the planet. The Lagrange points L4 and L5 lie in the planet's orbit, each forming an equilateral triangle with the planet and the Sun.

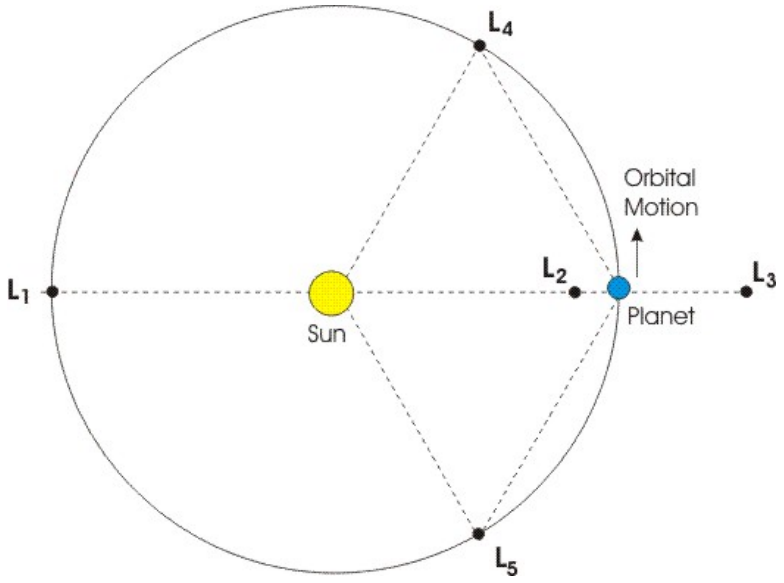

Figure 7. Stable Lagrange points formed by the Sun and an orbiting planet.

Because the satellites do not orbit the planet, perturbations due to atmospheric drag or planet triaxiality no longer affect a formation flying at a Lagrange point; however, solar radiation pressure effects remain important and must be corrected.

If it is not imperative for the array to remain in a given orbit, the formation can be sent into an Earth-trailing or fall-away heliocentric trajectory. In such cases the array will move away from its initial deployment location, following an orbital path shaped by the gravitational pull of the Sun and planets. The advantage of such a trajectory is that perturbations on the individual components of the array are negligible; the overall trajectory of the array will be gravitationally influenced by distant bodies, but these effects will not misalign the clustered satellites making up the array. Typical Earth-trailing orbits start at a distance of at least 1-AU from the Sun, the array will begin to trail the orbit of the Earth and will eventually move a significant distance away over the life of the mission. As such, the array cannot easily be recovered or serviced should malfunctions occur, and communication times with the array spacecraft will increase over the life of the mission. For both L2 and Earth-trailing orbits, the minor perturbations that might arise from solar radiation forces are significantly less severe than the various east-west and north-south station-keeping requirements that must be met by an array in Earth orbit.

A number of formation flying concepts have been developed to take advantage of the stability provided by Lagrangian orbits and heliocentric fall-away trajectories. Two representative concepts currently under review by NASA are the Terrestrial Planet Finder (TPF) mission, planned for launch in 2011, and the farther-term MAXIM x-ray interferometer mission. While neither is designed for use with shepherd satellites, they are used here to provide illustrative examples of how the shepsat concept might be applied for these kinds of missions. Section 3.5 below provides a brief overview of the TPF mission and the role shepherd satellites could play in missions of this type, while Section 3.6 discusses possible shepsat applications for the MAXIM array.

3.5 TPF and Formation-Flying Telescope Arrays

The Terrestrial Planet Finder (TPF) mission[4,56] is designed to characterize the size, temperature, and orbital parameters of extrasolar planetary systems out to a distance of 15 parsecs (approximately 50 light years). The array consists of a set of four collector spacecraft, each hosting a 3.5-m diameter mirror, and one combiner spacecraft; a nulling interferometer is used to combine the beams of the four collector spacecraft, reducing the light from the central star by a factor of at least 10^5 to allow the detection of potential planetary systems around the star. Over the five year mission of the TPF, approximately 150 star systems will be targeted in a search for planets as small as the Earth; spectroscopic follow up of 50 star systems will be performed to look for signs of atmospheric gases such as CO_2 and H_20, and more sensitive spectroscopic measurements will then be made of the 5 most promising systems to look for ozone, a byproduct of life. In addition to planetary searches, the TPF will also be used to study protoplanetary systems, star formation regions, and other astrophysical objects of interest.[‡]

The TPF will be launched either into L2 or, more probably, an Earth-trailing orbit. Starting in a helio-centric orbit of 1-AU, the array will eventually drift 0.6-AU from the Earth over its five-year mission life. The array baseline consists of the for collector spacecraft, uniformly spaced over a total baseline distance of 75 m to 1000 m, with the combiner spacecraft forming a coplanar isosceles triangle with the inner two collector spacecraft. An artist's sketch of the TPF is shown in Figure 8.

Figure 8. Terrestrial Planet Finder array.[4]

[‡] The European Space Agency is also evaluating a possible IR telescopic array mission, *DARWIN*, which like the TPF will search for terrestrial planets and signs of life in extrasolar systems as well as perform general astrophysical observations. For more information, see http://ast.star.rl.ac.uk/darwin.

For planetary observations, the TPF baseline will rotate 360^{o} every eight hours. For spectroscopic observations the array will rotate approximately 3^{o} per hour, while for astrophysical observations the requirements vary but will typically consist of a slow drift of the array baseline. Proposed propulsion systems to perform these maneuvers include hall thrusters and pulsed plasma thrusters, each of which are capable of providing the approximately 0.1-N of force required for rapid array acceleration. The positions of the array telescopes must be kept within 5-cm for fine pointing; pathlength drifts for the nulling interferometer are controlled using signals from lasers and accelerometers. The collector and combiner spacecraft masses are approximately 873 kg and 687 kg, respectively, including thrusters, propellant, and contingency mass. Additional information regarding the TPF mission, including science goals and technology requirements, can be found in the on-line TPF Handbook.[56]

3.5.1 Shepsat Options for TPF-Type Missions

The large masses of the four collector spacecraft and the requirement to rotate the array baseline once every eight hours would preclude the use of the shepherd satellite concept, which at 10^{-9} N/Watt cannot provide the required force of 0.1-N for each spacecraft with reasonable beam powers. Lower forces can be used, but they would increase the amount of time it takes to perform a given rotation or baseline maneuver and diminish the amount of observational time available in the limited duration mission. Nevertheless, this *type* of mission can still benefit from the use of shepsats by increasing the number and reducing the mass of the collector spacecraft. For example, rather than using four large (3.5-m) diameter mirrors, a similar mission might be performed using several smaller mirrors, reducing the mass of each collector and hence the amount of force required to position each satellite within the array. Instead of rotating the array to sweep out an observation path, a larger number of smaller collectors could be formed into an observing pattern (such as a cross) that would not require rotation, significantly simplifying the array control and propulsion requirements. Control of the coplanar collector and combiner spacecraft positions would be performed by shepherd satellites flying above and below the array; with no need to rotate the array, the restoring force and beam power requirements become much more reasonable (see Section 3.3.2 for a discussion of solar radiation correction requirements). The trade is in the increased complexity of the interferometry system used to null the light from the central star, but with accurate positioning of the collector spacecraft by the outrider shepsats this should be a manageable. Using shepherd satellites to position the collector and combiner spacecraft removes the requirement of on-board propulsion for the array components, reducing the total mass of each spacecraft and alleviating potential issues with mirror contamination by propellant plumes.

Potential issues with the use of shepsats for array control include the possible heating of the collector spacecraft mirrors by the microwave beams and the possibility of direct or scattered electromagnetic interference with spacecraft components or systems. Depending on the magnitude of the beam power and the required time on target for corrective positioning, the first problem can likely be addressed through proper passive cooling of the spacecraft. The second issue may be mitigated by the judicious selection of wavelengths for the radiation forces; microwave beams typically fall in the range of 10^{-1} m to 10^{-2} m, while the wavelengths chosen for TPF planetary detection are in the range of $7\text{x}10^{-6}$ to $2\text{x}10^{-5}$ m, and for general astrophysical observations they lie in the range from $3\text{x}10^{-6}$ m to $3\text{x}10^{-5}$ m. The disparity in wavelengths should prevent the control beams from directly interfering with the observations, and as noted above proper cooling of the mirrors should prevent temperature fluctuations due to beam absorption or reflection by spacecraft surfaces. Conversely, depending on the amount of time the beams need to illuminate a given spacecraft for position control, observations can be suspended during that period if interference effects are found to exist. Because the mission life is not limited by propellant mass, potential delays in target observation would not appear to be a serious issue.

While it remains to be investigated in detail, the shepsat concept appears to be a potentially viable candidate for the formation flying of telescopic arrays in L2 or Earth-trailing orbits, where a large number

of small mirrors in a fixed pattern can be controlled using electromagnetic gradient or scattering forces. Taking this concept to the extreme is the MAXIM x-ray interferometer, described in Section 3.7 below; unlike the smaller arrays discussed here, the MAXIM concept poses a distinct control challenge that the shepsat concept may not be able to meet.

3.6 The MAXIM X-Ray Interferometer Concept

The Micro-Arcsecond X-ray Imaging Mission (MAXIM)[9,57] began as a NIAC-sponsored research project to investigate the feasibility of achieving unprecedented x-ray astronomical images using a formation-flying x-ray interferometer. The concept has evolved to include a pathfinder mission, consisting of a single x-ray interferometer and a trailing imaging satellite, and the full MAXIM, consisting of a fleet of 33 x-ray mirror satellites, a trailing collector satellite, and an imaging or detector spacecraft. The full MAXIM concept is diagrammed below.

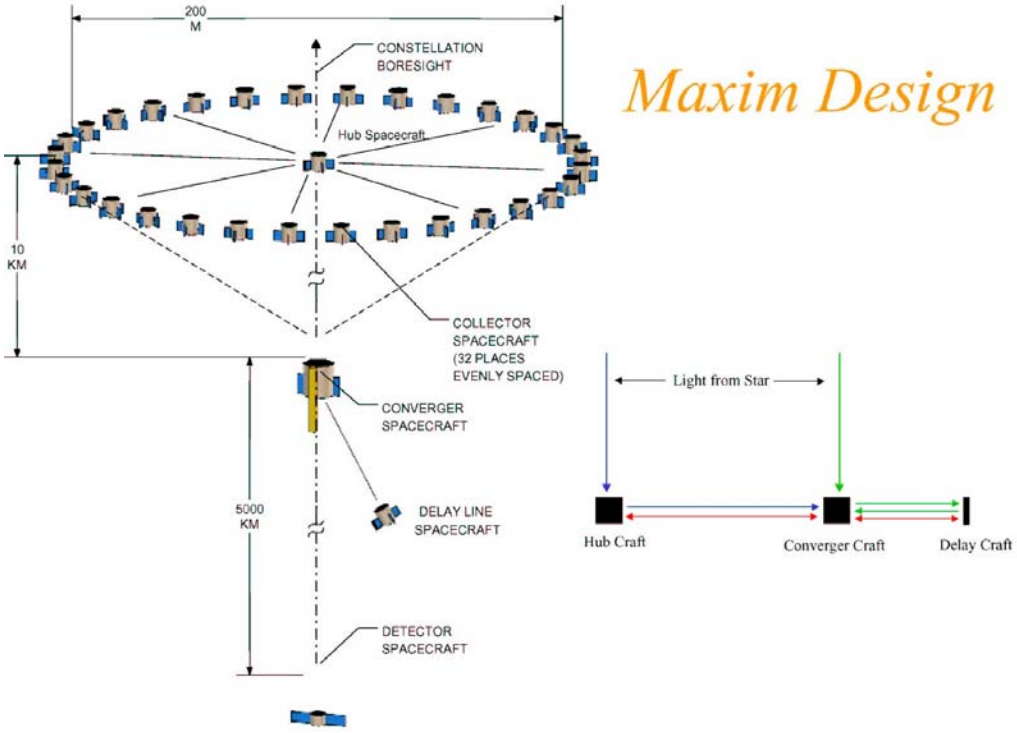

Figure 9. MAXIM formation-flying x-ray interferometer.[57]

As noted in the figure, 32 satellites are evenly space around a circular radius of 200-m to make up the x-ray collector portion of the interferometer, with an additional satellite stationed at the center of the circular formation to act as the array hub and provide the telescope bore line. A "converger" spacecraft, trailing the formation at a distance of approximately 10-km, acts as a secondary mirror to collimate the x-rays for a detector spacecraft, located an additional 5000-km downstream. As shown in the figure on the right, distant starlight is used to maintain a parallel path length and keep the formation aligned. With this configuration, it appears possible to image x-ray sources to within 100-nano-arcsecond resolution, sufficient to image the event horizon of black holes and other energetic galactic x-ray sources.

One of the principle challenges for this concept is to maintain the array positions of the collector spacecraft to within a few nanometers (10^{-9} m) over a radial distance of 200-m. This is an incredibly

daunting task, and one that has yet to be solved satisfactorily. Although most orbital perturbations are negligible in L2 orbits, solar radiation remains a potentially serious problem that can over time misalign the precise positions required of the collector spacecraft. Some form of on-board propulsion will be required, and the initial set of propulsion options considered by the MAXIM team included cold gas hydrazine thrusters, pulsed plasma thrusters, hall thrusters, electrostatic ion engines, and field emission electron propulsion systems.[58] The results indicated that none of the propulsion options were particularly attractive. Hydrazine thrusters had sufficient thrust for station-keeping, but the thrust was too high for attitude control and sloshing of the propellant in the tanks could seriously degrade the fine pointing accuracy required of the collector spacecraft. The pulsed plasma thruster also had adequate thrust and, with a solid propellant bar, eliminated the problem of propellant sloshing; however, the thrust was to high for attitude control applications, and as a repetitively pulsed electromagnetic system, there was concern about potential electromagnetic interference with command and control circuits on the collector spacecraft. The hall thruster can't be pulsed to provide fine attitude control, and as with the hydrazine thruster, propellant sloshing in the tanks could potentially degrade fine pointing control of the spacecraft. The same arguments were made with respect to the ion thruster. The FEEP system had sufficiently low thrust ($2\text{x}10^{-7}$ N) for accurate attitude control, but insufficient thrust for station-keeping. At this writing, a viable propulsion option for station-keeping the MAXIM collector spacecraft formation in an L2 orbit has not yet been determined. As part of the Phase I investigation of the shepherd satellite concept, an investigation was undertaken to determine whether electromagnetic radiation forces could provide the necessary restoring forces for the collector spacecraft. The results of that evaluation are discussed below.

3.6.1 MAXIM Station-Keeping Using Electromagnetic Forces

As discussed in Section 2.0, the magnitude of the radiation forces provided by electromagnetic scattering from a metallic surface or electromagnetic intensity gradients generated by interactions with a polarizable dielectric surface are on the order of 10^{-9} N per watt of incident beam power. For L2 orbits, this electromagnetic force must overcome the radiation pressure force caused by sunlight striking the surface of a spacecraft at approximately 1-AU. The perturbation acceleration, Δa, due to solar pressure acting on a satellite of mass M and surface area A is given by Equation 48, repeated below:

$$\Delta a = S(1+\sigma)\frac{A}{M}$$

where S is the solar constant at 1-AU, $4.5\text{x}10^{-6}$ kg/(m-s^2), and σ is the average reflectivity of the satellite. The perturbing solar radiation force is then given by $F_s = S(1+\sigma)A$, which must be compensated by the electromagnetic force provided by the shepherd satellite. The resulting force balance can be written as:

$$\frac{(10^{-9}\ \frac{N}{W})P(W)}{4.5\times10^{-6}\ \frac{kg}{m-s^2}} \geq (1+\sigma)A \qquad (53)$$

which reduces to

$$P(W) \geq 4.5\times10^{3}(1+\sigma)A \qquad (54)$$

The required beam power thus depends on the reflectivity and the size of the surface area of the collector spacecraft exposed to the sun. While these numbers have not yet been finalized, it appears reasonable to assume that the surface area will not exceed 2-m^2. Assuming a maximum reflectivity of unity, the maximum required beam power will be on the order of 18-kW per collector satellite. For an array of 32 collector spacecraft, the total required power is approximately 580-kW if all the collector satellites are to be simultaneously illuminated. For a lower reflectivity of 0.5 and a smaller surface area of 1-m^2, the

required power per beam is around 6.8-kW and the power required to simultaneously illuminate the total array is approximately 220-kW.

A possible technique to reduce the total beam power might be to sequentially illuminate each satellite in the array for a brief period of time, allowing it to drift between illumination periods. The acceleration predicted by Equation 48 for a 100-kg collector spacecraft with a 1-m^2 surface area and a reflectivity of 0.5 is approximately 6.8×10^{-8} m/s^2.* Assuming the perturbation is thus on the order of 10^{-7} m/s^2, the force required to hold a 100-kg spacecraft in place is around 10^{-5} N. If we wish to sequentially illuminate the 32 satellites in the array, we need to provide sufficient force during each illumination period to push the satellite slightly past it's equilibrium position and then allow it to drift back into position during the period of non-illumination. This implies that, for a 32-element array, we need 32 times more force during the brief period of illumination than we would require under continual illumination. For the example quoted above, the continual force required to hold one spacecraft in place against solar pressure is approximately 10^{-5} N, corresponding to a beam power of 10^4 W. If instead we choose to sequentially illuminate each satellite in turn, we require 32 times that beam power, or around 320-kW, to achieve the same effect. This is approximately the same order of magnitude in power that we require if we continually illuminate each satellite with a 10-kW beam, and it thus appears from a power perspective that there is no significant benefit in a sequential illumination of the array components. In addition, the tight positioning requirements for the MAXIM array would seem to preclude corrective maneuvers that would allow this type of drift-correct-drift approach.

3.6.2 MAXIM Central Shepsat Configuration

The first station-keeping geometry evaluated for the full MAXIM array considered the use of a single high power shepherd satellite centrally located at the array hub, with 32 lower power (~10-kW) individual microwave beams (one per collector satellite) continuously maintaining the satellite positions against solar radiation pressure. It was quickly realized that a single shepherd satellite located at the array center would be unable to maintain the circular nature of the array, for the following reason. Consider the array of collector spacecraft to lie in a plane parallel to the direction of the incident solar radiation (Figure 9). Depending on the orientation of the array with respect to the sun, part of the array will be pushed toward the hub while the other part will be pushed away from the hub. In this case, both scattering forces and gradient forces would be required to maintain the array position: for spacecraft lying between the sun and the hub, the microwave beam will push against the solar radiation force using electromagnetic scattering, while for spacecraft lying on the other side of the array, an intensity gradient force can be used to pull the spacecraft toward the focal point of the microwave beam. However, because the sun is a distant source, the solar radiation is nearly planar at the location of the array, pushing each satellite in the array in the same lateral direction. In contrast, the shepherd satellite located at the center of the array provides a radial restoring force, which introduces force components that no longer lie along the direction of the solar perturbation.

This problem is depicted in Figure 10, in which the solar illumination is presumed to come from the left side of the diagram. In the diagram, F_G represents gradient forces, F_S represents scattering forces, and there are eight representative collector spacecraft (blue) surrounding a single central shepherd satellite (red). As shown in the diagram, the radial scattering or gradient forces create additional force components on most of the collector spacecraft that will quickly distort the intended array shape. For collector spacecraft located in a direct line between the sun and the central shepherd satellite, the shepsat can accurately compensate for solar radiation perturbations without introducing spurious force components. For collector spacecraft located on a line perpendicular to the incident solar radiation, no combination of gradient or scattering forces from the centrally located shepherd satellite can compensate for the solar

* The size and mass of the collector spacecraft for the full MAXIM are not yet available on the project websites.

perturbation force. For spacecraft located between these two positions, the solar radiation force can be corrected but additional force components that arise from the applied radial forces will quickly distort the circular nature of the array. A single, centrally located shepherd satellite is thus insufficient to provide the restoring forces necessary to maintain the circular array of collector spacecraft making up the MAXIM array.

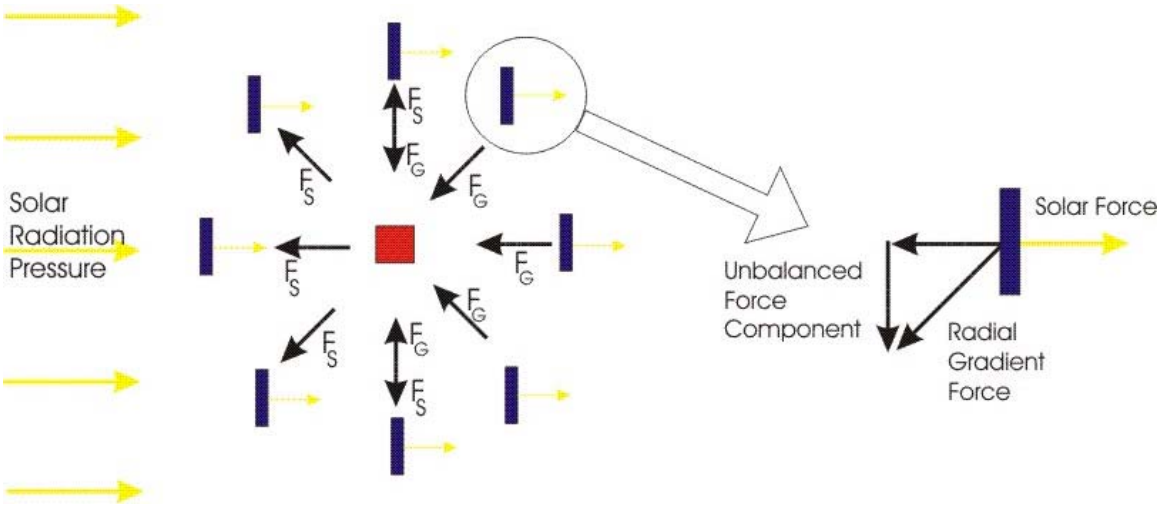

Figure 10. Force components due to centrally located shepherd satellite.

3.6.3 MAXIM Multiple Shepsat Configuration

To accurately compensate for the solar perturbations on the array, a set of shepherd satellites would have to be flown in formation with the collector spacecraft. A number of possible shepsat configurations were considered for this purpose, including a simple linear array bisecting the collector formation, a triad of shepsats lying in the same plane as the collector spacecraft, and multiple shepsats flying outside the MAXIM formation. The difficulty with each of these configurations lies in the inadvertent production and proper cancellation of electromagnetic force components perpendicular to the direction of the perturbing solar radiation force. After several attempts, the most promising arrangement appears to be a triangular formation of shepherd satellites flying in a plane perpendicular to the direction of the incident solar radiation, and located sunward of the collector array. A sketch of this configuration is shown in Figure 11.

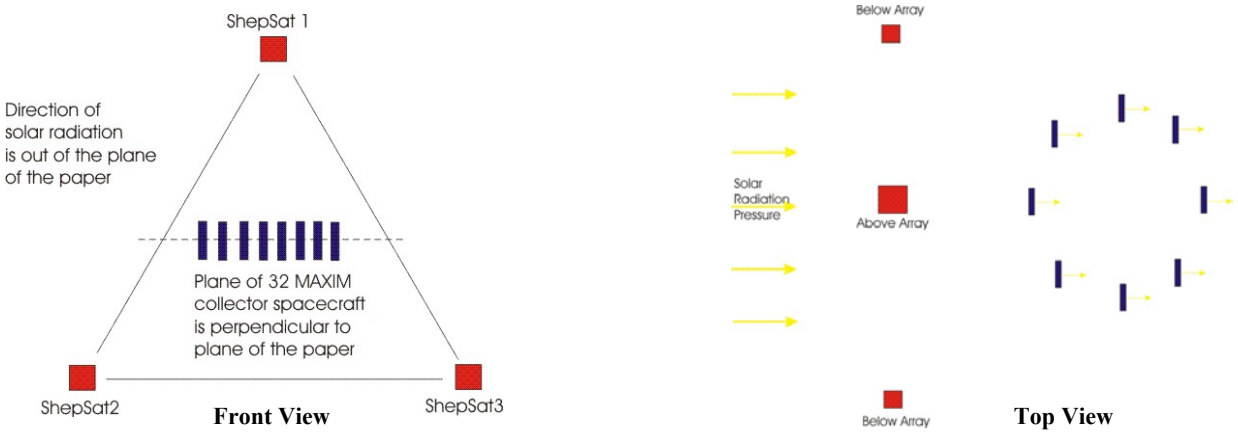

Figure 11. MAXIM collector spacecraft station-keeping with 3 shepherd satellites.

An evaluation of the gradient and scattering force vectors indicates that this 3-shepsat configuration is capable of providing the proper force components to compensate the solar radiation perturbations as well as cancel the additional force components that might otherwise alter the circular nature of the array. The arrangement also ensures that the shepsats have an unobstructed line of sight to each of the collector spacecraft in the array, no matter how steeply the collector array is tilted with respect to the plane of the shepherd satellites (as might occur during retargeting of the x-ray interferometer).

3.6.4 Issues with Station-Keeping the MAXIM Array

Because a minimum of two shepherd satellites are required to provide the continual illumination of several collector spacecraft to cancel the solar radiation forces and the unwanted electromagnetic components, each shepherd satellite will require fairly high (>100-kW) on-board power systems. Power can be generated using large solar panels attached the shepherd satellites or by more compact nuclear reactors located on extensible booms. Although the shepherd satellites will require on-board propulsion for station-keeping their triangular formation, the use of large solar arrays will exacerbate the problem of solar radiation pressure on the shepherd satellites and will require higher on-board thrust to hold the shepsats in place. A possible drawback to using a nuclear power source for the shepherd satellites is the potential generation of x-ray and gamma-ray radiation, which unless properly shielded could create additional background noise for the interferometer. Each of these issues will need to be considered in more detail, and a trade study performed to determine the least impact on the shepherd satellite and collection satellite arrays.

A second area of concern is the challenge of providing accurate on-board command and control to generate and point multiple microwave beams from each shepsat to hold the collector spacecraft in place. As noted above, two and sometimes three microwave beams will be required for each collector spacecraft to balance the solar radiation perturbations and electromagnetic force components, and for an array of 32 collector spacecraft, beam control becomes a fairly demanding control issue. Two factors mitigate this seemingly intractable problem. First, each microwave beam generated on a shepherd satellite can have it's own control logic for power and pointing, in essence making the shepherd satellite a high power host platform for a number of individual microwave transmitters. A single high power source can supply energy to a number of lower power microwave beam generators on each shepherd satellite, with each generator and corresponding antenna dedicated to a specific collector spacecraft. Because each beam is controlled independently and is dedicated to a single collector spacecraft, the required logic can potentially be much simpler than the logic required to sequentially illuminate each collector spacecraft with a single high power beam. The second mitigating factor is the use of continual illumination of the collector satellites. Because the collector array components are under constant illumination from the shepherd satellites, the beam strengths and focal points can be continuously adjusted to provide very fine positioning control. Knowledge of the collector spacecraft positions can be related to the central hub spacecraft in Figure 9, which in turn relays collector spacecraft position data to the shepherd satellites. While certainly not a simple system, the ability to provide autonomous on-board controls for continuous, individual beam power and steering appears at least feasible.

A third major issue is the focal spot size of the microwave beams used to provide the gradient forces depicted in Figure 11. To generate a gradient force, the focal spot of the beam must be accurately positioned a given distance in front of the dielectric target – presumed here to be a shell or external structure mounted to the collector spacecraft. The spot size for a Gaussian beam is given by the equation:[59]

$$2W_0 = \frac{4}{\pi}\lambda\frac{f}{D} \tag{55}$$

where W_0 is the is the focal spot radius, λ is the wavelength of the beam, f is the focal length of the focusing antenna (lens), and D is the antenna (lens) diameter. Because the shepherd satellites lie outside the array circumference, the distance from a given shepsat to a collector spacecraft on the far side of the array is a minimum of 200 m and is likely to be considerably larger; a typical value of the antenna focal length is thus taken to be around 300 m. If several microwave antennas are to be hosted on a single shepherd satellite, the physical dimensions of each antenna will of necessity be constrained to prevent the size of the shepherd satellite from becoming unwieldy; a reasonable diameter is taken to be 1-m.[†] The wavelength of a microwave beam is typically taken to range from 10^{-1} to 10^{-2} m; a value of 10^{-2} m will be used for this preliminary evaluation. Substituting the above values into Equation 55, the minim focal spot size for the microwave beam is around 3.8 meters. This implies that the location of the required intensity gradient will not be sharply defined, and the target spacecraft might only be held in place to within this level of accuracy. Clearly for an x-ray interferometry mission requiring nanometers of precision, the loose positioning indicated by this analysis will not suffice. The problem is less severe if scattering forces are used, with the shepherd spacecraft located on the opposite side of the array to the sun. However, unlike gradient forces, scattering forces alone may not be able to provide a stable equilibrium,[37] and as such it is not yet clear that the collector spacecraft can be held in position using purely scattering forces.

In summary, microwave-based shepherd satellites may not be able to control the position of the MAXIM collector spacecraft with sufficient precision for x-ray interferometry applications. While beam power and control issues can be adequately addressed, the required placement of the shepherd satellites outside the array will result in large focal spot sizes that diminish the sharpness of the intensity gradients and reduce the accuracy with which the collector spacecraft can be positioned within the array. Additional research must be performed to determine if there is a suitably stable equilibrium configuration using electromagnetic scattering forces instead of gradient forces; this can be carried out once the details of the MAXIM satellites are better determined.

3.7 Life Finder Mission

The NIAC-funded *Life Finder* concept proposed by Wolf and colleagues[10] consists of a large area, non-circular, high angular resolution telescope that will collect detailed atmospheric spectra of any extrasolar terrestrial planets discovered by the predecessor Terrestrial Planet Finder (TPF) mission (see Section 3.5). The collecting area of the Life Finder telescope will be in the range of 500 m^2 to 5000 m^2, compared to a total collecting area of approximately 50 m^2 for the TPF array. The Life Finder mission would search for firm evidence of life on candidate planets by analyzing constituents of the atmosphere that can only be caused by biological processes, looking for methane and other gases that TPF cannot detect. Instead of the nulling interferometer used by TPF, Life Finder will use a coronagraph to block the light of the central star in the planetary system. In addition, the proposed mirror shape is not circular but rather elongated, with full images built up by rotating the mirror about its axis. Because mirror cooling and vibration damping issues are critical, Life Finder will be placed in a heliocentric fall-away orbit and will not use on-board propulsion for positioning or reaction wheels for pointing. Instead, the telescope will use a set of louvers on a sun-shade mounted behind the telescope to provide a reaction-less, solar-radiation torque to rotate the telescope. While this concept alleviates most of the major damping issues associated with on-board propulsion or reaction wheels, the motion of the actuated louvers will create some vibration in the structure, as will the onset and termination of rotation if the telescope mass is not properly distributed. While it is not clear how the actual pointing of the telescope at different targets will be accomplished, it appears that the telescope may be mounted to a mechanical elbow on the sun-shade boom, which could also lead to mechanical vibrations. The Life Finder team calculates that for a typical space structure with

[†] For example, an antenna matrix could consist of five rows with five 1-m diameter antennas per row to provide a total of 25 antennas in an approximate 5m x 5m space. Beam steering can be accomplished by scanning the smaller focusing elements, without the need to physically move the more bulky main antennas.

a Q of 1000, if a 10-Å level of vibration is incurred after positioning, and a level of 1-Å is required for wavefront accuracy, then approximately 12 exponential decay times are required, or roughly 10^4 times the resonant period of the telescope. If the resonant period is 1-s, then the telescope will have to settle for approximately 2.8 hours before an observation can be made, each time the telescope is positioned. This in turn requires that the telescope have a period of at most a fraction of a second to prevent unwarranted delays in observing time. The team is considering ultra-light load bearing frames and actuator driven glass optics for a prototype mini-Life Finder mission, but a full Life Finder mission will likely require a thin membrane under tension; the higher the tension, the higher the resonance frequency and the faster the damping of any vibrations. Electrostatic forces are suggested as a means of slightly curving the membrane surface, providing a convergent beam for collection by a free-flying collector spacecraft located at the focal point of the telescope.

While this is a decidedly far-term mission, a preliminary evaluation was performed to assess what role the shepsat concept might play in enhancing or enabling this type of mission. Ideally, there should be no driven mechanical forces acting on the structure, and hence no need to constrain the telescope design to mitigate possible vibration effects. As such, rather than use actuator-driven louvers on a sun-shade to provide rotation or a mechanical joint for mirror positioning, it might be possible to achieve the same effect with applied radiation forces provided by formation flying shepherd satellites. For example, it may be beneficial to have the solar shade unattached from the telescope, making it a free-flyer that can be repositioned to provide maximum mirror coverage as new planets are examined. It would be convenient to have a separate on-board propulsion system to maneuver the shade, but if there is a concern about propellant plume effects it would also be possible to use electromagnetic radiation forces provided by nearby shepherd satellites to keep the shade and telescope flying in the proper formation. Rather than using actuator driven solar louvers on a shade attached to the telescope to provide rotation of the telescope, the torque required by the elongated telescope mirror to sequence an image could be accomplished using target handles radially mounted at the telescope center of mass; electromagnetic gradient forces can be used to gently “pull” on a handle and initiate rotation, while scattering forces from the same shepsat can be used to slowly “push” on the handle and stop rotation. Illuminating other target handles mounted along the axis of the telescope could provide accurate yaw and pitch motions, without the need for vibration-inducing mechanical systems or any actual physical contact with the free-flying telescope. An array of shepherd satellites could be on-station to provide full three-dimensional positioning of the telescope mirror, illuminating various handles to position and point the telescope as the free-flying sun-shield provides thermal cover from solar illumination. Such an arrangement would virtually eliminate problems with structural vibration, while providing a full range of motion for unrestricted observational access. Some of the potential issues that would need to be addressed include the optimum placement of the target handles to smoothly control the motion of the telescope, possible thermal interactions between the microwave beams and the target material, the possible transmission of heat from the target handles to the telescope body, and potential interactions between the microwave beams and telescope systems. Still, the use of applied non-solar radiation forces for telescope rotation and pointing control might be worth considering as research continues on the Life Finder mission.

3.8 Summary of Potential Mission Applications

As shown in the preceding sections, the shepsat concept for formation flying arrays is clearly not applicable in all instances; satellite masses may be too large for the electromagnetic radiation force provided, orbital perturbations may be too severe, or array position tolerances too demanding. However, the ability to use beamed electromagnetic radiation to manipulate and control structures in space does offer a new, potentially robust technique for formation flying low-mass arrays in Earth orbit, or station-keeping simple spacecraft formations in L2 or heliocentric fall-away orbits. Following is a brief summary of the potential shepsat mission applications considered in this report:

- LEO. The application of shepsats in LEO falls into two categories. At altitudes below 1000-km, the radiation forces generated by the shepherd satellites are probably too weak to counter atmospheric drag forces for all but the smallest nanosatellites. For larger satellites in this regime, the shepsats can perhaps best be used as on-orbit beacons to provide a reference frame for microsatellites making up the formation-flying array. A microwave beam on board the shepsat could repeatedly and precisely illuminate each location in the desired formation; using an intensity sensor, each microsatellite adjusts its position to remain at the local intensity spot generated by the beam. Although this requires each microsatellite to carry a propulsion system to overcome drag and other orbital perturbations, it significantly reduces the complexity associated with locating and managing a free-flying formation using ground commands. Above 1000-km, the radiation forces provided by the shepherd satellites are sufficient to overcome atmospheric drag for most microsatellites of interest. In this regime of operation the shepsats can actually provide drag makeup to hold the microsats in precise formation, without requiring on-board propulsion for each microsatellite. This would allow the microsatellites to dedicate more of their limited mass and power to instrumentation or other payloads in place of thrusters and propellant; however, if the array is to be repositioned, the micro-satellites would still require on-board propulsion to perform orbit maneuvers in a reasonable amount of time. In such instances, the microsatellites would be repositioned using on-board propulsion systems to a new orbital location, with the shepsat microwave beams providing a formation (intensity) reference frame. Once in place, the microsat propulsion systems would be shut off and orbit perturbations would again be compensated using scattering or gradient radiation forces from the shepsat microwave beams. The advantage of this technique again lies in the simplicity of using a few on-orbit shepsats to provide array guidance and control of several formation-flying microsatellites, in place of a complex command and control system to station-keep the array.

- MEO. Drag forces are less severe in medium earth orbit, and the proposed concept can compensate for atmospheric drag above approximately 1000-km. Other orbital perturbations due to solar radiation pressure and earth triaxiality effects can readily be compensated. Changes in inclination can be corrected for small (~10-kg) microsatellite masses, but larger satellites may require on-board propulsion to assist in north-south station keeping.

- GEO. Without a restoring force, each microsatellite in the formation-flying array will undergo a change in inclination due to sun-moon perturbations of approximately 0.85^{o} per year. Based on analytic predictions of the microwave radiation forces, the proposed shepsat concept can adequately supply north-south station keeping for small (<10-kg) microsatellites using reasonable beam powers (<15-kW per microsatellite). However, the concept will probably not be able to provide sufficient acceleration to overcome north-south perturbations for significantly larger microsatellites, since the required power per beam increases linearly with satellite mass. Thus for larger satellites (>10-kg), auxiliary propulsion will be probably be required for north-south station keeping of the array. East-west perturbations due to solar radiation pressure and Earth triaxiality perturbations can be readily compensated by the proposed shepsat concept using modest microwave beam powers.

- L2 and Earth-Trailing Orbits. The primary perturbation faced by formation-flying arrays located at a stable Lagrangian point or following an Earth-trailing, heliocentric orbit is solar radiation pressure. The shepsat concept appears well suited to provide radiative force corrections for simple formation flying arrays at these locations, and may in some instances be used to point and position array components. The smooth, continual application of radiative forces would reduce the structural vibrations produced by intermittent thruster firings as well as mitigate plume contamination of mirrors or other array components, both of which are important for TPF-type deep space astronomical arrays. However, due to the relatively long wavelength of the corrective microwave beams the focal spot for radiative gradient force corrections may not be sufficiently precise for more demanding

applications such as x-ray interferometry, and the use of radiative scattering forces alone may not provide a suitably stable array configuration. Still, the use of shepherd satellites to control formation-flying arrays in Lagrangian or Earth-trailing orbits appears to be a very promising avenue for further research.

While not an exhaustive review of potential applications, the results outlined above indicate that the relative simplicity offered by the shepherd satellite concept compared to more complex on-board or ground-to-space command and control schemes for array control could in many cases provide an innovative, robust technique for future formation-flying arrays. Although a significant amount of work remains to be done, the basic concept of using radiation forces provided by shepherd satellites to control an array of smaller microsatellites is feasible, and is one which may one day enhance or enable a number of new formation flying missions.

4.0 Microwave Sources and Beam Steering

A preliminary review was undertaken of microwave power sources, antenna designs, and beam steering techniques for potential application in the shepherd satellite concept. The purpose of the review was not to develop a full microwave beam system design, but rather to evaluate the current state of commercial microwave power generation and propagation to better assess the feasibility of providing the beam powers and steering capabilities required by the shepsat concept. This limited review did not include military microwave systems, which are expected to provide significantly enhanced performance as they are transitioned into commercial applications over the coming decades.

4.1 Microwave Power Sources

It is presumed that the electrical power for the microwave beams will be provided by solar arrays mounted to the shepherd satellites. Based on the required shepsat capabilities outlined in prior monthly reports, microwave beam powers of a few kW up to approximately 10-kW are sufficient to provide the electromagnetic radiation forces necessary for microsatellite array control. Even considering the possible need to provide several simultaneous microwave beams, these power levels are not excessive and the solar array requirements are not anticipated to be a major impediment to the shepherd satellite concept.

The conversion of electrical energy into microwave beam energy can be accomplished through a variety of devices. The principle commercial technologies capable of producing continuous, kW-class microwave power levels include klystrons, magnetrons, traveling wave tubes, and, for longer mm-wavelengths, gyrotrons.[60-63] Commercial magnetrons, such as the devices used to power microwave ovens, are compact, low mass, high power devices capable of delivering up to 100-kW of continuous microwave power. Klystrons and traveling wave tubes are typically larger in size and more massive, while gyrotrons are still fairly experimental in nature. Any of these technologies can be used to provide the required beam powers for the shepsat concept, though magnetrons currently have the edge as compact, high power, low mass sources. For example, the IMG-915-75k magnetron manufactured by ISTOK, Inc.[64] has a mass of approximately 8-kg and provides 75-kW of continuous power at 915-MHz. A set of two magnetrons mounted in a single shepherd satellite would provide ample power for multiple 10-kW beams, or provide for a limited set of higher power beams that could be used to reduce the time on target. The low mass of even present-day magnetrons will allow redundant power sources to be stored on-board the shepsats, significantly reducing mission risk and extending operational lifetime. While an extensive survey of current commercial capabilities has not been completed, microwave power generation does not appear to be a major hurdle for the shepsat concept.

4.2 Microwave Antennas and Beam Steering

Once the microwave power is generated, it needs to be directed by an antenna to either uniformly scatter off the microsatellite surface for an electromagnetic "push", or to be focused at a specified distance ahead of the microsatellite to create an intensity gradient and corresponding electromagnetic "pull". There are a number of techniques available to form and transmit microwave beams, several of which are analogous to the familiar beam formation and propagation methods used at optical electromagnetic frequencies. While a detailed derivation of the shepherd satellite antenna design is beyond the scope of the present Phase I activity, the following summaries provide a brief overview of several possible techniques:[65-67]

4.2.1 Parabolic Antenna and Lens Systems

The microwave power generated by a magnetron or similar device can be fed through a highly efficient waveguide to a horn antenna located at the focal point of a reflecting parabolic dish. The microwave radiation emitted by the horn is reflected from the parabolic dish into a parallel beam, which can then be focused using dielectric microwave lenses. Variations on the parabolic antenna include Gregorian and Cassegranian systems, in which radiation from a feed horn located behind the main parabolic dish is passed through an opening in the dish and reflected from a small secondary reflector located at the focal point. The radiation reflected from secondary reflector is collimated upon reflection from the primary dish to provide a parallel microwave beam. In Gregorian systems the secondary reflector has an elliptic shape, while in Cassegranian systems the secondary reflector is hyperbolic. Once the beam is formed, a dielectric lens or set of lenses can be used to shape the beam and bring it to a focal point at the required distance, in direct analogy to the focusing of an optical beam by transparent lenses. Scanning of the microwave beam can be performed either by slewing the parabolic reflector and lens combination, or by more advanced techniques in which the secondary reflector is turned to scan the beam location. Polarization of the microwave beam for gradient force interactions is achieved by passing the beam through a metal grating or set of gratings to produce the desired polarization direction. There are a large number of such well-established techniques for designing and using parabolic reflectors and dielectric lenses for microwave and millimeter wave beam formation and propagation, and these current methods can be directly applied to the proposed shepherd satellite concept.

4.2.2 Adaptive Antennas

A far-term concept for beam steering and focusing involves the use of deformable primary reflectors. While this has not yet been developed for microwave systems, research is underway to develop such systems at optical wavelengths.[68] In this concept, actuators mounted to the underside of the reflector surface are used to change the radius of curvature of the primary parabolic reflector, providing a variable focal length without the need for additional lenses. Such a system would significantly reduce the mass associated with a mirror/lens combination, and combined with mechanical beam steering the resulting variable reflector system would provide a potentially robust alternative to the standard parabolic reflectors outlined above.

4.2.3 Phased Arrays

A significant amount of research over the past few decades has gone into the development of phased array antennas. As its name implies, the phased array antenna consists of individual microwave radiators arranged in either a linear or two-dimension pattern; the amplitude and phase of each radiator is individually controlled to form a radiated beam of any given shape. The direction of the resulting beam can be changed by electronically adjusting the phase of the individual antenna elements, allowing the beam to be scanned without moving the antenna system. High microwave beam power can be achieved by distributing several lower power generators across the phased array aperture, potentially improving

system life and reliability by mitigating the need for a single high power source. The unique beam control afforded by combining individual array elements provides significant flexibility in beam steering and focus, and despite the increased complexity, phased array antennas appear to be very well suited for the shepsat concept.

In summary, techniques currently exist to form and propagate a microwave beam at the power levels required for the shepherd satellite concept. It is anticipated that future advances in microwave power sources, conformable reflectors, and phased array antennas will provide even more compact, high power, highly directional microwave beam propagation systems, and as such microwave power generation and beam formation do not appear to be major issues for the proposed concept.

4.3 Beam Interactions with Microsatellites

The microwave beam transmitted from the shepherd satellite must interact with the target microsatellite to provide an electromagnetic force sufficient to either overcome orbital perturbations and keep the satellite in a fixed position within the formation-flying array, or to change the location or orientation of the satellite with respect to the other array members. As described in Section 2.0, the two radiation forces under consideration are (i) scattering forces, in which the microwave beam is reflected from the microsatellite to push the satellite in the direction of the beam, and (ii) gradient forces, in which the beam is focused at a point away from the satellite to provide an interaction between the electromagnetic field and an induced dipole within the microsatellite surface that draws it toward the focal point of the beam. Based on the calculations presented in this report, typical microwave beam powers will need to be on the order of a few to several kilowatts, incident on the spacecraft for several minutes to several hours, depending on the magnitude of the perturbation that must be suppressed. As discussed in Section 3.5, heating of the microsatellite surface by direct interaction with the microwave beam and possible electromagnetic interference with sensitive spacecraft instruments and electronics are potential concerns. Other complications may arise when the disparate nature of surface materials are taken into account; for near-Earth applications, the compact microsatellites will likely be powered by solar cells affixed to the satellite body, and the potential non-uniformity of the surface materials may produce uneven forces that give rise to undesired force components. Additional problems arise if the solar arrays are mounted on a deployable boom, which will alter the preferred symmetric nature of the microsatellite surface.

To mitigate these potential beam interactions issues, it is proposed that thin dielectric shells be mounted circumferentially around the microsatellite body using insulated stand-offs, at a radius slightly larger than the satellite radius. The dielectric shells can be made highly reflective at microwave wavelengths if scattering forces are to be used, or they can be made of a suitable microwave dielectric material if gradient forces are the primary force interaction. In either instance, optically transparent materials can be employed so as not to block the transmission of solar radiation to photovoltaic cells. For example, open mesh metallic gratings can be used to provide microwave reflection for scattering forces, while solid materials such as optically transparent quartz could be used to provide a suitable microwave dielectric material for gradient force interactions.[69,70] The shells can be left open at each end to provide unobstructed viewing access to instruments and sensors. While just a preliminary concept, the use of stand-off shells to provide uniform surfaces for beam-satellite interactions appears to solve a number of potential issues regarding microsatellite surface heating and equipment interactions, and should be considered as part of any future design efforts.

5.0 CONCLUDING REMARKS AND RECOMMENDATIONS

Based on the results of this preliminary Phase I effort, it appears that the proposed shepherd satellite concept for station-keeping an array of smaller microsatellites is indeed feasible. Radiation forces on the order of 10^{-9} N/W may be generated using electromagnetic gradient forces or scattering forces; microwave beam powers of 10-kW can thus produce restoring forces of approximately 10-μN, which are sufficient to correct a number of orbital perturbations. Potential applications where the shepsat concept could play a significant role include drag makeup for linear arrays in Earth orbit, at altitudes exceeding 1000-km; East-West and North-South station-keeping of large nanosatellite arrays in geosynchronous Earth orbit; and the cancellation of solar radiation forces acting on arrays located at the Lagrangian points or in heliocentric, fall-away orbits. While a substantial amount of work remains to be done, the concept offers an innovative, viable approach for the control of future formation-flying arrays.

The following research areas are recommended to provide additional insights into the uses and limitations of the proposed shepherd satellite concept.

Recommendations for Further Research:

Advanced Numerical Models

- The shepsat radiation forces upon which the mission applications are based were developed from analytic radiation force models in the optical wavelength regime; these must be rigorously extended into the microwave regime, and numerical models must be developed to accurately determine the range of interactions between the incident beams and the microsatellites.

The analytic models that have been published to date evaluate laser beam optical trapping of particles using two approximations: geometric optics for dielectric Mie particles, and electromagnetic wave theory for dielectric and metallic Rayleigh particles. While these analytic models provide a general level of agreement with experiments, numerical models are required to better understand and quantify the radiation forces expected to act on the array microsatellites. Based on the shepherd satellite mission applications presented in Section 3.0 (*Shepherd Satellite Mission Applications*), the Mie-particle approximation appears to be a reasonable start for more rigorous numerical modeling the radiation forces expected to act on the microsatellite arrays. It is assumed that the wavelength of the electromagnetic radiation beamed from the shepsats will be significantly smaller than most foreseeable microsatellite or nanosatellite dimensions, and this approximation satisfies the use of microwaves to generate and transmit the required beam intensities. To further refine the modeling effort, it can be assumed that if intensity gradient forces are to be employed, the microsatellites can be modeled as an ideal dielectric by offsetting a thin dielectric shell around the circumference of the microsatellite; if mainly scattering forces are to be considered, the dielectric shell can be replaced with a highly reflective metal shell to enhance the reflection coefficient. Numerical models developed by Gussgard, Lindmo and Brevik[41] and Ke and Gu[42] appear to satisfy these constraints, and provide general guidance on algorithm development to calculate scattering and gradient forces in the Mie regime. As such, these models could be used as a starting point to develop numerical models that might better predict the radiation forces that can be generated by a focused microwave beam interacting with a microsatellite.

Experimental Force Validation

- It is strongly recommended that a future research effort include an experimental demonstration of microwave gradient forces and scattering forces to verify the predicted radiation forces, allowing a more accurate assessment of the proposed concept.

The analytic models have been extended from optical wavelengths, in which a number of confirmatory experiments have been performed, to microwave wavelengths, where to date no electromagnetic trapping experiments have been reported. It is necessary to perform experiments that will validate the current analytic models and the future numerical simulations that will be used to model microsatellite interactions with microwave radiation forces. A suggested approach is to perform these experiments in a suitably large vacuum chamber; a microwave source placed at one end of the chamber can be used to illuminate a suspended target, using either focused radiation to provide gradient force interactions or planar radiation to provide scattering forces. The target can consist of a simple mass surrounded by either a dielectric shell (gradient forces) or a reflective shell (scattering forces); deflections of the suspended mass from vertical correlate to the strength of the imposed electromagnetic force. This technique allows a number of radiation force effects to be evaluated as a function of various parameters, such as variations in beam power, beam shape, change in focal point location, dielectric strengths, reflectivity, target mass, and material surface shape. Evaluating both the gradient and scattering radiation forces over such a wide parameter range would provide ample experimental data for code validation, and would provide some measure of confidence in the ability of shepherd satellites to station-keep future formation flying arrays.

ACKNOWLEDGEMENTS

Funding for this Phase I research effort was provided by the NASA Institute for Advanced Concepts (NIAC) under grant 07600-072. The author thanks NIAC Director Dr. Robert Cassanova and the NIAC staff for their comments and support during the performance of this grant.

REFERENCES

1. National Aeronautics and Space Administration (NASA,) *Strategic Plan*, link at www.nasa.gov.
2. Bristow, J., Bauer, F., Hartman, K., and How, J., "Enabling Spacecraft Formation Flying Through Position Determination, Control and Enhanced Automation Technologies", NASA Technical Report 2000-0086214, Jan 2000.
3. For an up to date description of the Space Technology 3 mission, see http://nmp.jpl.nasa.gov/st3.
4. For an up to date description of the Terrestrial Planet Finder mission, see http://tpf.jpl.nasa.gov.
5. Salomonson, V., "An Overview of Future NASA Missions, Concepts, and Technologies Related to Imaging of the World's Land Areas", NASA Technical Report 1999-0106568, Jan 1999.
6. For up to date information on the European Space Agency missions, see http://sci/esa.int/content.
7. Wilson, J. R., "Satellite Clusters Reshape Space Plans", *Aerospace America*, pp 27-30, Nov 2000.
8. Das, A., "Choreographing Affordable, Next-Generation Space Missions Using Satellite Clusters", *AFRL Technology Horizons*, pp 15-16, Sep 2000.
9. Cash, W., "X-ray Interferometry", presented at the NIAC Fellows Meeting, June 2001, NASA Ames Research Center, CA; published at http://www.niac.usra.edu/studies.
10. Woolf, N., "The Path to Lifefinder", published at http://www.niac.usra.edu/studies.
11. Beckey, I., "An Extremely Large Yet Ultralightweight Space Telescope and Array", Phase I final report, May 1999, published at http://www.niac.usra.edu/studies.
12. Ticker, R. and Azzolini, J., "2000 Survey of Distributed Spacecraft Technologies and Architectures for NASA's Earth Science Enterprise in the 2010-2025 Timeframe", NASA Technical Report 2000-0091540, Aug 2000.
13. Folta, D., Newman, L. K., and Quinn, D., "Design and Implementation of Satellite Formations and Constellations", NASA Technical Report 1998-0237734, Jan 1998.
14. Bayard, D. S. and Burdick, G. M., "Deep Space Control Challenges of the New Millennium", NASA Technical Report 2000-0068537, January 1999.

15. Long, M. R. and Hall, C. D., "Attitude Tracking Control for Spacecraft Formation Flying", NASA Technical Report 1999-0064184, May 1999.
16. Bauer, F. H., Bristow, J. O., Carpenter, J. R., Garrison, J. L., Hartman, K., Lee, T., Long, A., Kelbel, D., Lu, V., How, J. P., and Busse, F., "Enabling Spacecraft Formation Flying in Any Earth Orbit Through Spaceborne GPS and Enhanced Autonomy Techniques", NASA Technical Report 2000-0031724, Dec 2000.
17. Folta, D., Carpenter, J. R., and Wagner, C., "Formation Flying with Decentralized Control in Libration Point Orbits", NASA Technical Report 2000-0083880, Jan 2000.
18. Mesbahi, M. and Hadaegh, F. Y., "A Robust Control Approach for the Formation Flying of Multiple Spacecraft", NASA Technical Report 2000-0056090, Jan 2000.
19. Mesbahi, M. and Hadaegh, F. Y., "Reconfigurable Control for the Formation Flying of Multiple Spacecraft", NASA Technical Report 2000-0054885, Jan 2000.
20. Lorenz, R., "Small Satellites and Electric Propulsion – a Review", *Aeronautical Journal*, pp 204-213, June/July 1991.
21. Gagosian, J. S., Rhee, M. S., and Zakrzwski, C. M., "Nanosatellite Propulsion Development Program", NASA Technical Report 1999-0032065, January 1999.
22. Rayburn, C., Campbell, M., Hoskins, W., and Cassady, R., "Development of a Micro Pulsed Plasma Thruster for the Dawgstar Nanosatellite", AIAA 2000-3256, presented at the 36th Joint Propulsion Conference, Huntsville, AL, July 2000.
23. Gulczinski, F., Dulligan, M., Lake, J., and Spanjers, G., "Micropropulsion Research at AFRL", AIAA 2000-3255, presented at the 36th Joint Propulsion Conference, Huntsville, AL, July 2000.
24. Hoskins, W. A. and Cassady, R. J., "Applications for Pulsed Plasma Thrusters and the Development of Small PPTs for Microspacecraft", AIAA-2000-3434, presented at the 36th Joint Propulsion Conference, Huntsville, AL, July 2000.
25. Johnson, L., Gilchrist, B., Estes, R. D., and Lorenzini, E., "Overview of Future NASA Tether Applications", NASA Technical Report 1998-0237034, Jan 1998.
26. Quinn, D., and Folta, D., "A Tethered Formation Flying Concept for the SPECS Missions", NASA Technical Report 2000-0032752, Jan 2000.
27. Omori, R., Kobayashi, T., and Suzuki, A., "Observation of a Single-Beam Gradient Force Optical Trap for Dielectric Particles in Air", *Optics Letters*, 22 (11), pp. 816-818, June 1997.
28. Svoboda, K. and Block, S., "Optical Trapping of Metallic Rayleigh Particles", *Optics Letters*, 19 (13), pp. 930-932, July 1994.
29. Tlusty, T., Meller, A., and Bar-Ziv, R., "Optical Gradient Forces of Strongly Localized Fields", *Phys Rev Letters*, 81 (8), pp. 1738-1741, Aug 1998.
30. Sato, S., Harada, Y., and Waseda, Y., "Optical Trapping of Microscopic Metal Particles", *Optics Letters*, 19 (2), pp. 1807-1809, Nov 1994.
31. Zemanek, P., Jonas, A., Sramek, L., and Liska, M., "Optical Trapping of Nanoparticles and Microparticles by a Gaussian Standing Wave", *Optics Letters*, 24 (21), pp. 1448-1450, Nov 1999.
32. Ashkin, A., Dziedzic, J. M., Bjorkholm, J. E., Chu, S., "Observation of a Single-Beam Gradient Force Optical Trap for Dielectric Particles", *Optics Letters*, 11 (5), 1986, pp. 288-290.
33. Ashkin, A., "Acceleration and Trapping of Particles by Radiation Pressure", *Physical Review Letters*, 24 (4), 1970, pp. 156-159.
34. Ashkin, A. and Dziedzic, J. M., "Optical Levitation in High Vacuum", *Applied Physics Letters*, 28 (6), pp. 333-335.
35. Svoboda, K. and Block, S., "Optical Trapping of Metallic Rayleigh Particles", *Optics Letters*, 19 (13), 1994, pp. 930-932.
36. Sato, S., Harada, Y., and Waseda, Y., "Optical Trapping of Microscopic Metal Particles", *Optics Letters*, 19 (22), pp. 1807-1809, 1994.
37. Ashkin, A. and Gordon, J. P., "Stability of Radiation-Pressure Particle Traps: An Optical Earnshaw Theorem", *Optics Letters*, 8 (10), pp. 511-513, Oct 1983.

38. Harada, Y. and Asakura, T., "Radiation Forces on a Dielectric Sphere in the Rayleigh Scattering Regime", *Optics Communications*, 124, 1996, pp. 529-541.
39. Stratton, J. A., Electromagnetic Theory, McGraw-Hill, New York, 1941.
40. Wright, W. H., Sonek, G. J., and Berns, M. W., "Parametric Study of the Forces on Microspheres Held by Optical Tweezers", *Applied Optics*, 33 (9), 1735-1748.
41. Gussgard, R., Lindmo, T., and Brevik, I., "Calculation of the Trapping Force in a Strongly Focused Laser Beam", *J. Opt. Soc. Am. B*, 9 (10), 1992, pp. 1922-1930.
42. Ke, P. C. and Gu, M., "Characterization of Trapping Force on Metallic Mie Particles", *Applied Optics*, 38 (1), pp. 160-167, Jan 1999
43. Gautheir, R. and Ashman, M., "Simulated Dynamic Behavior of Single and Multiple Spheres in the Trap region of Focused Laser Beams", *Applied Optics*, 37 (27), pp. 6421-6431, Sep 1998.
44. Kim, J. and Kim, S., "Dynamic Motion Analysis of Optically Trapped Nonspherical Particles with Off-Axis Position and Arbitrary Orientation", *Applied Optics*, 39 (24), pp. 4327-4333, Aug 2000.
45. Ke, P. and Gu, M., "Characterization of Trapping Force on Metallic Mie Particles", *Applied Optics*, 38 (1), 1999, pp. 160-167.
46. Zemanek, P., Jonas, A., Sramek, L., and Liska, M., "Optical Trapping of Rayleigh Particles Using a Gaussian Standing Wave", *Optics Communications*, 151, 1998, pp. 273-285.B
47. Barton, J. P. and Alexander, D. R., "Fifth-Order Corrected Electromagnetic Field Components for a Fundamental Gaussian Beam", *J. Applied Physics*, 66 (7), 1989, pp. 2800-2802.
48. Barton, J. P., Alexander, D. R., and Schaub, S. A., "Theoretical Determination of Net Radiation Force and Torque for a Spherical Particle Illuminated by a Focused Laser Beam", *J. Applied Physics*, 66 (10), 1989, pp. 4594-4602.
49. Davis, L. W., "Theory of Electromagnetic Beams", *Physical Review A*, 19 (3), 1979, pp. 1177-1179.
50. Gousbet, G., Maheu, B., and Grehan, G., "Light Scattering from a Sphere Arbitrarily Located in a Gaussian Beam, Using a Bromwich Formulation", *J. Opt. Soc. Am. A*, 5 (9), 1988, pp. 1427-1443.
51. Ren, K. F., Grehan, G., and Gousbet, G., "Prediction of Reverse Radiation Pressure by Generalized Lorenz-Mie Theory", *Applied Optics*, 35 (15), 1996, pp. 2702-2710.
52. Zombeck, M. V., Handbook of Space Astronomy and Astrophysics, Cambridge University Press, Cambridge, 1982, p. 161.
53. Hedin, A. E., "Extension of the MSIS thermospheric model into the middle and lower atmosphere, *Journal of Geophysical Research*, Vol. 96, pp. 1159-72, 1999. Also see Ketsdever, A. D., Wong, J., and Reed, H., "A University Microsatellite as a MEMS-Based Propulsion System", AIAA-2000-3670, presented at the 36th Joint Propulsion Conference, Huntsville, AL, 16-19 July 2000.
54. Ketsdever, A. D., Wong, J., and Reed, H., "A University Microsatellite as a MEMS-Based Propulsion System", AIAA-2000-3670, presented at the 36th Joint Propulsion Conference, Huntsville, AL, 16-19 July 2000.
55. Lovell, R. and O'Malley, T., "Station Keeping of High Power Communication Satellites", NASA TM X-2136, August 1973.
56. The on-line TPF Handbook is located at http://tpf.jpl.nasa.gov/library/tpf_book/index.html.
57. Cash, W., "Micro-Arcsecond X-ray Imaging Mission", published at http://maxim.gsfc.nasa.gov.
58. Grady, J., First Definition Team Meeting, published at http://maxim.gsfc.nasa.gov.
59. Saleh, B. and Teich, M., Fundamentals of Photonics, J. Wiley and Sons, Inc., NY, 1991, pp.92-97.
60. Thomas, H., Handbook of Microwave Techniques and Equipment, Prentice-Hall, Inc., Englewood Cliffs, NJ, 1972.
61. Gandhi, O., Microwave Engineering and Applications, Pergamon Press, New York, 1981.
62. Coleman, J., Microwave Devices, Reston Publishing Co., Prentice Hall, Inc., Reston, VA, 1982.
63. Ishii, T. K., Microwave Engineering, 2nd edition, Harcourt Brace Jovanovich, Inc., San Diego, 1989.
64. The referenced magnetron data sheet is available at www.istok.com; additional performance and mechanical properties of a large variety of microwave sources are readily obtained through an Internet search using the following keywords: magnetron; klystron; traveling wave tube; gyrotron.
65. Cornbleet, S., Microwave Optics, Academic Press, New York, NY, 1976.

66. Johnson, R. C., (ed), Antenna Engineering Handbook, 3rd Ed., McGraw-Hill, Inc., New York, 1993.
67. Balanis, C., Antenna Theory: Analysis and Design, 2nd Ed, J. Wiley & Sons, Inc., New York, 1997.
68. Boghosian, M. and Tang, W., "Magnetically Actuated Miniature Paraboloidal Mirrors with Variable Radii of Curvature", *NASA Tech Briefs (Photonics)*, October 2001, p 13a.
69. Saad, T., Hansen, R., and Wheeler, G., editors, Microwave Engineers Handbook, Vol. 2, Artech House, inc., Dedham, MA, 1971.
70. Thomas, H., Handbook of Microwave Techniques and Equipment, Prentice-Hall, Inc., 1972.

Appendix A

Calculation Of Atmospheric Drag Based on User Supplied Inputs

```
C     DRAG CALCULATIONS FOR SMALL SATELLITES

      DIMENSION RHOHIGH(9),RHOLOW(9)

C     ESTIMATED ATMOSPHERIC MASS DENSITY VS. ORBIT (KG/M^3)
      RHOLOW(1)=2.E-10     !200 KM
      RHOHIGH(1)=5.E-10
      RHOLOW(2)=1.E-11     !300 KM
      RHOHIGH(2)=7.E-11
      RHOLOW(3)=5.E-12     !400 KM
      RHOHIGH(3)=1.E-11
      RHOLOW(4)=6.E-14     !500 KM
      RHOHIGH(4)=1.E-12
      RHOLOW(5)=1.E-14     !600 KM
      RHOHIGH(5)=5.E-13
      RHOLOW(6)=3.E-15     !700 KM
      RHOHIGH(6)=1.E-13
      RHOLOW(7)=2.E-15     !800 KM
      RHOHIGH(7)=5.E-14
      RHOLOW(8)=1.E-15     !900 KM
      RHOHIGH(8)=2.E-14
      RHOLOW(9)=9.E-16     !1000 KM
      RHOHIGH(9)=8.E-15

C     RANGE FOR ATMOSPHERIC DRAG COEFFICIENTS
      CDMIN=2.0
      CDAVG=2.2
      CDMAX=4.0

      RE=6378.5  !KM; EQUATORIAL EARTH RADIUS

500   WRITE(6,*) 'SATELLITE MASS (KG): '
      READ(6,*) SCMASS
      WRITE(6,*) 'ORBIT RADIUS (200<=R<=1000 KM): '
      READ(6,*) RADIUS
      IF((RADIUS.LT.200.).OR.(RADIUS.GT.1000)) THEN
        WRITE(6,*) 'ENTER ORBIT RADIUS (200<=R<=1000): '
        READ(6,*) RADIUS
      END IF
      TOTRAD=(RADIUS+RE)*1000.  !CONVERT TO METERS
      RADIUS=RADIUS*1000. !HEIGHT ABOVE SURFACE
      WRITE(6,*) 'SATELLITE CROSS-SECTIONAL AREA (M^2): '
      READ(6,*) AREA

      VCIRC=(1.996E7)/SQRT(TOTRAD) !CIRCULAR ORBIT VELOCITY
      WRITE(6,*) ' '
```

```
      WRITE(6,*) 'CIRCULAR ORBITAL VELOCITY (M/S): ',VCIRC

      BMIN=SCMASS/(CDMAX*AREA)
      BAVG=SCMASS/(CDAVG*AREA)
      BMAX=SCMASS/(CDMIN*AREA)

      WRITE(6,*) '  MINIMUM BALLISTIC COEFFICIENT: ',BMIN
      WRITE(6,*) '  TYPICAL BALLISTIC COEFFICIENT: ',BAVG
      WRITE(6,*) '  MAXIMUM BALLISTIC COEFFICIENT: ',BMAX

C     ESTIMATE ATMOSPHERIC MASS DENSITY:
      XRAD=(RADIUS/1.E5)-1.0
      IRAD=INT(XRAD+0.6)
      DENMIN=RHOLOW(IRAD)
      DENMAX=RHOHIGH(IRAD)
      WRITE(6,*) 'MINIMUM ATMOSPHERIC DENSITY (KG/M^3): ',DENMIN
      WRITE(6,*) 'MAXIMUM ATMOSPHERIC DENSITY (KG/M^3): ',DENMAX

      DRAGVAL=0.5*SCMASS*(VCIRC**2)*1000. !USED IN DRAG CALCULATIONS
                                          !CONVERTS TO mN FORCE
C     ESTIMATED RANGE OF DRAG FORCE:
      WRITE(6,*) ' '
      WRITE(6,*) 'ATMOSPHERIC DRAG CALCULATIONS '
      WRITE(6,*) '   MINIMUM ATMOSPHERIC DENSITY:'
      DRAG1=DRAGVAL*DENMIN/BMAX
      WRITE(6,200) DRAG1
      DRAG2=DRAGVAL*DENMIN/BMIN
      WRITE(6,210) DRAG2
      DRAG3=DRAGVAL*DENMIN/BAVG
      WRITE(6,220) DRAG3

      WRITE(6,*) '   MAXIMUM ATMOSPHERIC DENSITY:'
      DRAG1=DRAGVAL*DENMAX/BMAX
      WRITE(6,200) DRAG1
      DRAG2=DRAGVAL*DENMAX/BMIN
      WRITE(6,210) DRAG2
      DRAG3=DRAGVAL*DENMAX/BAVG
      WRITE(6,220) DRAG3

      WRITE(6,*)
      WRITE(6,*) 'RUN AGAIN? (1/Y,0/N): '
      READ(6,*) IRUN
      IF(IRUN.EQ.1) GOTO 500
      WRITE(6,*) 'PROGRAM TERMINATED'

200   FORMAT(' MINIMUM DRAG FORCE (mN): ',F8.4)
210   FORMAT(' MAXIMUM DRAG FORCE (mN): ',F8.4)
220   FORMAT(' TYPICAL DRAG FORCE (mN): ',F8.4)

      STOP
      END
```

APPENDIX B

Atmospheric Drag Calculation for Range of Orbital Altitudes and Cross Sectional Areas

```
C       PARAMETRIC DRAG CALCULATIONS FOR SMALL SATELLITES

        DIMENSION RHOMAX(9),RHOMIN(9),CD(5),SCMASS(7),ORBIT(9),
     &          AREA(8),VEL(9)

        OPEN(1,FILE='DRAGDATA.DAT',FORM='FORMATTED',STATUS='NEW')

C     ESTIMATED ATMOSPHERIC MASS DENSITY VS. ORBIT (KG/M^3)
          RHOMIN(1)=2.E-10      !200 KM
          RHOMAX(1)=5.E-10
          RHOMIN(2)=1.E-11      !300 KM
          RHOMAX(2)=7.E-11
          RHOMIN(3)=5.E-12      !400 KM
          RHOMAX(3)=1.E-11
          RHOMIN(4)=6.E-14      !500 KM
          RHOMAX(4)=1.E-12
          RHOMIN(5)=1.E-14      !600 KM
          RHOMAX(5)=5.E-13
          RHOMIN(6)=3.E-15      !700 KM
          RHOMAX(6)=1.E-13
          RHOMIN(7)=2.E-15      !800 KM
          RHOMAX(7)=5.E-14
          RHOMIN(8)=1.E-15      !900 KM
          RHOMAX(8)=2.E-14
          RHOMIN(9)=9.E-16      !1000 KM
          RHOMAX(9)=8.E-15

C     RANGE FOR ATMOSPHERIC DRAG COEFFICIENTS
          CD(1)=2.0
          CD(2)=2.5
          CD(3)=3.0
          CD(4)=3.5
          CD(5)=4.0

C     RANGE FOR SPACECRAFT MASS (KG)
          SCMASS(1)=1.0
          SCMASS(2)=5.0
          SCMASS(3)=10.0
          SCMASS(4)=25.0
          SCMASS(5)=50.0
          SCMASS(6)=75.0
          SCMASS(7)=100.0

C     RANGE FOR SPACECRAFT AREA (DIRECTION OF MOTION; M^2):
          AREA(1)=0.1
          AREA(2)=0.2
```

```
      AREA(3)=0.3
      AREA(4)=0.4
      AREA(5)=0.5
      AREA(6)=0.75
      AREA(7)=1.0
      AREA(8)=2.0

C     RANGE FOR ORBITAL RADIUS (KM):
      ORBIT(1)=200.
      ORBIT(2)=300.
      ORBIT(3)=400.
      ORBIT(4)=500.
      ORBIT(5)=600.
      ORBIT(6)=700.
      ORBIT(7)=800.
      ORBIT(8)=900
      ORBIT(9)=1000.

C     RANGE FOR ORBITAL VELOCITY (FNCN OF ALTITUDE; M/S)
      DO 10 I=1,9
      VEL(I)=(1.996E7)/SQRT((ORBIT(I)+6378.5)*1000.)
10    CONTINUE

C     ****BEGIN CALCULATION LOOPS****

C     LOOP 1 OVER SPACECRAFT MASS:

      DO 100 I=1,7
      WRITE(6,*) 'SPACECRAFT MASS (kg): ',SCMASS(I)


C     LOOP 2 OVER SPACECRAFT AREA:
      DO 110 J=1,8
      WRITE(1,600)
      WRITE(1,700) SCMASS(I)
      WRITE(1,710) AREA(J)
      WRITE(1,600)

C     LOOP 3 OVER CIRCULAR ORBIT ALTITUDE:
      WRITE(1,720)
      DO 120 K=1,9

C     LOOP 4 OVER DRAG COEFFICIENTS
      DO 130 L=1,5

C     CALCULATIONS:

C      BALLISTIC COEFFICIENT:
      BCOEF=SCMASS(I)/(AREA(J)*CD(L))

C      MINIMUM DRAG FORCE FOR GIVEN BALLISTIC COEFFICENT:
```

```
      FMIN=(0.5*RHOMIN(K)*SCMASS(I)*(VEL(K)**2))/BCOEF
      FMAX=(0.5*RHOMAX(K)*SCMASS(I)*(VEL(K)**2))/BCOEF

C     WRITE DATA FILES:
      WRITE(1,730) ORBIT(K),VEL(K),FMIN*1000.,FMAX*1000.

130   CONTINUE
120   CONTINUE
110   CONTINUE
100   CONTINUE

600   FORMAT(' ****************')
700   FORMAT(' SPACECRAFT MASS: ',F8.4,' kg')
710   FORMAT(' SPACECRAFT AREA: ',F8.4,' m^2')
720   FORMAT(' ORBIT(km)',4X,'VELOCITY(m/s)',5X,'FMIN(mN)',8X,
     &          'FMAX(mN)')
730   FORMAT(1X,F8.2,5X,1PE12.6,4X,1PE12.6,4X,1PE12.6)

      CLOSE(1)
      WRITE(6,*) 'PROGRAM TERMINATED'

      STOP
      END
```

Appendix C

Perturbation Correction Code

```
C       EVALUATE APPLIED FORCE REQUIREMENTS TO COUNTER DRAG
C       AND KEEP MICROSATELLITE WITHIN SPECIFIED DISTANCE

        OPEN(1,FILE='FORCEDAT.DAT',FORM='FORMATTED',STATUS='NEW')

500     WRITE(6,*) 'ENTER ALLOWABLE DRIFT DISTANCE (M): '
        READ *, ZVAL
        WRITE(6,*) 'ENTER DRAG FORCE (N): '
        READ*,DRAG
        WRITE(6,*) 'ENTER APPLIED FORCE (N): '
        READ*, APPLIED
        WRITE(6,*) 'ENTER MICROSATELLITE MASS (KG): '
        READ*, SATMASS
        WRITE(6,*) 'ENTER TIME STEP (SEC): '
        READ*, DELTIME

C       START WITH APPLIED FORCE OFF
C       ALLOW TO DRIFT TO -ZMAX/2, THEN BRING BACK TO +ZMAX/2

        ZMIN=-ZVAL/2.           !LOWER BOUNDARY ON ALLOWED DRIFT
        ZMAX=ZVAL/2.            !UPPER BOUND ON ALLOWED DRIFT
        DRIFT=0.0               !INITIAL DRIFT DISPLACEMENT
        TIME=0.0                !INITIAL TIME = 0.0

        DO 10 I=1,1000
        WRITE(1,*) TIME/3600., DRIFT
        WRITE(6,*) TIME/3600., DRIFT
 100    TIME=TIME+DELTIME
        DRIFT=DRIFT-(DRAG*DELTIME**2)/(2.*SATMASS)
        IF(DRIFT.LE.ZMIN) THEN
        DO 20 K=1,1000
        TIME=TIME+DELTIME
        WRITE(6,*) TIME/3600., DRIFT
        DRIFT=DRIFT+(APPLIED-DRAG)*(DELTIME**2)/(2.*SATMASS)
        WRITE(1,*) TIME/3600., DRIFT
        IF(DRIFT.GE.ZMAX) GO TO 100
20      CONTINUE
        END IF
10      CONTINUE

        WRITE(6,*) 'RUN AGAIN? (1=Y/0=N): '
        READ*, IRUN
        IF(IRUN.EQ.1) GO TO 500

        CLOSE(1)
        STOP
        END
```